Characterization of Brillouin Scattering Spectrum in LEAF Fiber

by

Xuan Liu

Thesis submitted to the
Faculty of Graduate and Postdoctoral Studies
In partial fulfillment of the requirements
For the M.Sc. degree in Physics

Department of Physics
Faculty of Science
University of Ottawa

Table of Content

List of Figures

List of Tables

List of Abbreviations

ASE:	Amplified Spontaneous Emission
BGS:	Brillouin Gain Spectrum
BOCDA:	Brillouin Optical Correlation Domain Analysis
BOFDA:	Brillouin Optical Frequency Domain Analysis
BOTDA:	Brillouin Optical Time Domain Analysis
BOTDR:	Brillouin Optical Time Domain Reflectometry
CD:	Chromatic Dispersion
DCF:	Dispersion Compensating Fibers
DGD:	Differential Group Delay
DSF:	Dispersion Shifted Fiber
EFPI:	Extrinsic Fabry Perot Interferometer
EOM:	Electro-optic Modulator
ESA:	Electrical Spectrum Analyzer
FBG:	Fiber Bragg Gratings
FUT:	Fiber Under Test
GVD:	Group Velocity Dispersion
IFPI:	Intrinsic Fabry Perot Interferometer
ITU:	International Telecommunication Union
LEAF:	Large Effective Area Fiber
NZDSF:	Non-zero Dispersion Shifted Fiber

OPGW:	Optical Ground Wire
OTDR:	Optical Time Domain Reflectometry
PCF:	Photonic Crystal Fiber
PDF:	Probability Density Function
PM:	Polarization Maintaining
PMD:	Polarization Mode Dispersion
PSP:	Principle State of Polarization
SBS:	Stimulated Brillouin Scattering
SHM:	Structural Health Monitoring
SMF:	Single-mode Fiber
SNR:	Signal to Noise Ratio
SOP:	State of Polarization
V_B:	Brillouin Frequency Shift

Abstract

Fiber optic sensors are designed to measure various parameters. The distributed fiber optics sensor has been a very promising candidate for the structural health monitoring. In this thesis, we characterized LEAF (Large Effective Area Fiber) fiber's Brillouin scattering spectrum and investigated its potentiality for the distributed Brillouin temperature and strain sensor.

Optical fibers with complex refractive index profiles are applied to improve the Brillouin threshold by varying the Brillouin linewidth. As LEAF fiber has a modified refractive index profile, we investigated its Brillouin linewidth's dependence on the square of the pump light's frequency. We verified the Brillouin frequency's variation with input SOP experimentally for LEAF fiber in the spontaneous regime. This sets a limitation for the frequency resolution of distributed Brillouin sensors. We also realized a simultaneous temperature and strain sensor with LEAF fiber applying the Brillouin optical time domain analysis. Based on the direct detection of LEAF beat frequencies, a simultaneous strain and temperature sensor was demonstrated.

Acknowledgements

It is my pleasure to take this opportunity to thank all the people who have helped me over the past two years.

I would like to thank my supervisor Dr Xiaoyi Bao who has given me the opportunity to be a member of the fiber optics group at the University of Ottawa. Her passion in research and the critical thinking guided me through my master's study. I acquired many precise and rigorous methods and experience on how to conduct a good research project from her insightful instruction. Her diligence and innovative spirit have set a good example for me. This thesis would be impossible without her constant support and discussions. I also want to thank Dr Liang Chen for his help and suggestions in the theoretical part of my research. I was impressed and inspired by his strict work ethic and profound knowledge in the theory of fiber optics.

My colleagues in the fiber optics group have given me many assistance when I started the research. I wish to thank Dr. Wenhai Li who has helped me to configurate a BOTDA system, Dr. Yongkang Dong and Mr. Shangran Xie for their stimulating discussion and suggestions.

Finally, I must thank my parents and my younger brother. Their encouragement, understanding and constant love made this work possible.

Statement of Originality

This work contains no material which has been accepted for the award of any other degree or diploma in any university or other tertiary institution and, to the best of my knowledge and belief, contains no material previously published or written by another person, except where due reference has been made in the text.

I give consent to this copy of my thesis, when deposited in the University Library, being available for loan and photocopying.

SIGNED:……..

DATA:……

Supervisor: Prof. Xiaoyi Bao

Chapter 1

Introduction

Stimulated Brillouin scattering (SBS) is one of the areas of nonlinear optics which has gained great development with hundreds of papers published annually [1]. In this thesis, we focus the research on the two most recent advances of SBS in optical fibers applying LEAF fiber: SBS suppression in high-power fiber laser and amplifier designs and SBS-Based fiber optic sensors. This chapter gives the background and contributions of the thesis. Section 1.1 and 1.2 introduces fiber optic sensors and the structural health monitoring (SHM) where the distributed fiber optic sensors are a promising candidate. Section 1.3 and 1.4 present the thesis's contribution and outline respectively.

1.1 Fiber Optic Sensors

Fiber Optic Sensors can be designed to measure or sense almost anything: rotation, linear and angular position, acceleration, electric and magnetic field, temperature, strain, pressure, vibration, acoustics, humidity, liquid level, viscosity, and chemical measurements. There are many kinds of sensor designs including Bragg, Intrinsic Fabry Perot Interferometer (IFPI) and Extrinsic Fabry Perot Interferometer (EFPI). Compared to established conventional sensors, fiber optic sensors have the advantages of being

lightweight, having a very small size, requiring lower power, having a higher sensitivity, having a wider bandwidth and being immune to electromagnetic interference. Thanks to the development in the industries of optoelectronic and fiber optic communication, the ability of fiber optic sensor to replace more traditional point sensors has been enhanced.

There are many types of fiber optic sensors. The simplest one is based on intensity modulation [2] [3]. This method has the disadvantage that there are losses in the system not resulting from the variables to be measured. These losses were caused by microbending loss, macrobending loss, splices and connectors and misalignment between light sources and detectors. To circumvent this problem spectrally based fiber optic sensors were developed. Here, the light beam's wavelength was modulated by the environmental effects. Examples of these types of fiber were those based on blackbody radiation, absorption, etalons, fluorescence and dispersive grating. The development of high performance interferometeric fiber optic sensor has been one of the areas of intense interest. Research on Mach-Zehnder and Michelson interferometers, Sagnac interferometers and ring resonators has been undertaken.

Most fiber optic sensors such as the Fiber Bragg Gratings (FBG) and EFPIs that are available commercially are still point sensors same as the conventional sensors. If we take the Bragg gratings for strain sensing as an example, the gratings have to be put in certain locations where the strain is to be measured. Employing the techniques of time, frequency, wavelength, coherence, polarization and spatial multiplexing, it is possible to realize large numbers of sensors being supported by one single fiber optic line. Time division multiplexing is usually applied to design the distributed sensors where the strain,

temperature or other parameters are collected. In this technique a pulsed light source is launched into an optical fiber and the information from different positions are discriminated by analyzing the time delay. This method is utilized in Brillouin optical time domain analysis (BOTDA). A distributed sensor is able to measure the parameters continuously at all points within the sensing medium.

1.2 Structural Health Monitoring

Public civil structures such as railways, bridges, roads, tunnels, dams have become a vital part of our society. However, they may be subjected to bad changes in their structural health conditions due to overloads, natural disasters like earthquakes, potential damage induced by errors in design and construction and their normal working life [4]. The sudden collapse of structures will bring about many repairs, costs and even the loss of human lives. These tragedies can be found all over the world. Therefore, it is demanded to assess the structural health conditions so as to prevent disasters, reduce risks and perform maintenance activities optimally.

The most promising technique for optical fiber sensors suitable for SHM applications is the distributed sensor. In these sensors, optical fibers attached to or embedded inside the material act simultaneously as the optical channel and the distributed optical transducer. Currently, Rayleigh scattering, Brillouin scattering and Raman scattering are all explored for use in combination with optical reflectometric and signal processing techniques [5]. Applying Optical Time Domain Reflectometry (OTDR)

the Rayleigh-scattered light can be utilized to measure the attenuation profiles of long-haul fiber-optic links [6]. By recording the ratio between the anti-Stokes and Stokes sidelobes of the Raman scattering spectrum, the Raman scattered light is used for temperature distributed sensors [5]. In 1989, Brillouin scattering was proposed for the first time to measure temperature [7]. Since the Stokes sidelobe is sensitive to both temperature and strain, this method is now exploited for distributed temperature and strain sensing.

1.3 Thesis Contributions

A recently discovered overlap integral [8] between the electric and acoustic fields which was initially ignored by the conventional SBS theory [9] was introduced to reduce the SBS (more details can be found in section 2.4) by reducing this value. For the conventional step index optical fiber the overlap integral is about 1. However, this value can be reduced by designing the refractive index profiles to change the optical and acoustic fields [10] [11] [12]. It was shown in [8] that a non-zero dispersion shifted fiber (NZDSF) had a higher SBS threshold than the SMF with a step index profile. As will be introduced in section 2.1, LEAF fiber is one type of the NZDSF. Since the optical fibers with tailored acoustic profiles are critical for SBS suppression, the research of the linewidth's dependence on different wavelengths of the input pump light becomes important. We took LEAF fiber as one of the examples and for the first time studied its Brillouin frequency dependence at 1310nm and 1550nm.

The distributed Brillouin sensor is based on the sensitivity of the Brillouin frequency shift on both temperature and strain. This induces a problem of separating the effect of temperature from strain. Many methods have been proposed to solve this problem. The most recent solutions were applying the multi-peak spectrum of special fibers due to the different dependence of each peaks' Brillouin frequency shift on temperature and strain. LEAF fiber is one of these examples. We characterized LEAF fiber's Brillouin spectrum and realized the simultaneous temperature and strain measurement using the first peak's Brillouin frequency and linewidth measurement.

In distributed Brillouin scattering measurements, a lot of contributions have been made to improve the frequency resolution which determines the temperature and strain resolution. The conventional frequency accuracy is related to the linewidth and signal to noise ratio (SNR) [13]. However, the effective refractive index change which is induced by the varying polarization in optical fibers also causes the change of the Brillouin frequency shift. Thus, the frequency resolution should also affected by the polarization effect in the optical fiber. We discussed this issue and measured the value of the Brillouin peak frequency and Brillouin linewidth change range when the input SOP was tuned 97 times.

Except for high frequency resolution, high spatial resolution and long sensing length are also required in SHM. Therefore, in addition to BOTDA and Brillouin Optical Time Domain Reflectometry (BOTDR), other Brillouin distributed fiber optic sensors were also developed: they are the Brillouin optical frequency domain analysis (BOFDA) [14] [15] and the Brillouin optical correlation domain analysis (BOCDA) [16] [17] [18], both

used to improve the spatial resolution. These configurations are not only complicated but also time consuming. A new method applying the LEAF beat spectrum was introduced for the Brillouin strain and temperature sensor. It has the advantage of faster measurement time, simpler system configuration and much cheaper cost since it uses standard communication fiber (which is cheaper than Photonic Crystal Fiber (PCF) and other specially designed fiber) and single laser operation.

1.4 Thesis Outline

The thesis contains seven chapters and is organized as follows.

Chapter 2 introduces the different fiber types, the physics of light scattering in optical fibers and SBS suppression. These are the foundations of the whole thesis.

Chapter 3 studies the linewidth's dependence on pump light's wavelength of LEAF fiber, which is related to the SBS threshold suppression.

Chapter 4 focuses on the simultaneous temperature and strain measurement using LEAF fiber for the distributed Brillouin sensor system.

Chapter 5 corrects the frequency resolution's limitation in traditional Brillouin sensor by taking into account the polarization effect.

Chapter 6 proposes a new method using the LEAF beat for Brillouin temperature and strain sensor, which would simplify the normal Brillouin sensor configurations significantly.

In chapter 7, the conclusion and future work are given to the entire thesis.

Chapter 2

Scattering in Optical Fibers

This chapter introduces different optical fibers, the principles of light scattering and the motivation and methods for SBS suppression. The chapter is organized as follows. Section 2.1 presents some popularly used optical fibers and the purpose of designing them. Section 2.2 demonstrates all types of light scattering and their physics in optical fiber. Section 2.3 discusses the spontaneous and stimulated Brillouin scattering in details. Section 2.4 introduces SBS suppression and the existing methods to realize it.

2.1 Fiber Types

In optical communication systems, some popular fiber types that are often used have been standardized by the International Telecommunication Union (ITU). The standard single-mode fiber (SMF) which is known as the ITU-T G.652 fiber is the most commonly used fiber in long distance optical communication systems. An example of this type of fiber is Corning SMF-28^{TM}. This fiber has a simple step-index structure with a 8.2-μm core diameter and a 125-μm cladding diameter. The refractive index profile is shown in fig 2.1(a). Its zero dispersion wavelength is 1313 nm while the typical chromatic dispersion (CD) value at 1550 nm is about 17 ps/nm-km.

Although the SMF is suitable for long-distance optical communications due to its low loss at the 1550nm wavelength window, its relatively high chromatic dispersion around this wavelength induces significant waveform distortion at high speed (>10Gb/s) fiber communication systems.

Because of this the dispersion-shifted fiber (DSF) was developed to shift the zero-dispersion wavelength from 1310 nm to around 1550 nm so that the 1550 nm wavelength had both the lowest loss and dispersion. However, it was found that there existed large nonlinear crosstalk between different channels when there were many wavelengths propagating.

So the NZDSF were introduced to move the zero-dispersion wavelength near to but outside the 1550nm window. For this kind of fiber, the CD around 1550nm is smaller than SMF but larger than DSF. As a result, it not only reduces CD but also the nonlinear crosstalk at 1550nm. LEAF (large effective area fiber) fiber is one of this fiber. It is known for its larger core sizes than the common NZDSF whose core sizes are usually smaller than standard SMF. Its CD around 1550nm is about 4ps/nm-km while at 1310nm the value is about -22ps/nm-km. The maximum fiber attenuation at 1550nm is 0.2dB/km.

Apart from the already mentioned fibers which are designed for optical transmission, there are also various specialty fibers for optical signal processing. The examples are: polarization maintaining (PM) fibers, PCF, dispersion compensating fibers (DCF), and rare-earth doped active fibers for optical amplification.

In the distributed Brillouin sensors, the standard single mode fiber is most commonly used. Recently, LEAF fiber and other special fibers have also been applied in

the simultaneous temperature and strain measurement of distributed Brillouin sensors, which will be discussed in detail in chapter 4.

2.2 Light Scattering

The general spectrum of the scattered light for spontaneous light scattering is illustrated in fig 2.1. There are four different types of scattering: Raman, Brillouin, Rayleigh, and Rayleigh-wing. Those parts which are shifted to higher frequencies are the anti-Stokes components while those have lower frequencies are the Stokes components. Here, υ_o is the input light's frequency while I_s is the scattered light's intensity.

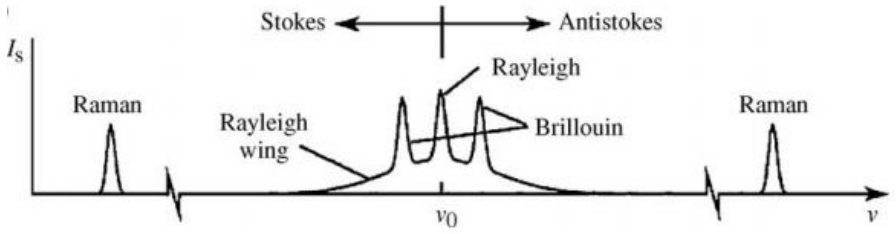

Fig 2. 1. Typical spontaneous light scattering spectrum [19]

The interaction of light with the vibrational modes of the molecules in the scattering medium leads to Raman scattering. It can also be regarded as the scattering of light from optical phonons. The scattering of light from sound waves (propagating pressure waves) results in Brillouin scattering. It can be described as the scattering of light from acoustic phonons. The scattering of light from non-propagating density fluctuations produces Rayleigh scattering (or Rayleigh-center scattering). Since it induces no frequency shift, it is also known as quasi-elastic scattering. The scattering from fluctuations in the

orientation of anisotropic molecules induces Rayleigh-wing scattering. This component's spectrum is very broad due to the rapid molecular reorientation process. For molecules with an isotropic polarizability tensor, Rayleigh-wing scattering does not occur. The frequency shift of the Brillouin Stokes and anti-Stokes components compared to the Rayleigh peak is the Brillouin frequency shift V_B.

2.3 Spontaneous and Stimulated Brillouin Scattering

Since our research focuses on Brillouin backscattered light, only this scattering process will be described in details.

In the macroscopic description of the light scattering, spontaneous Brillouin scattering happens as the result of fluctuations in the dielectric constant which results from the fluctuations in thermodynamic variables such as the material density and temperature.

For spontaneous Brillouin scattering, the equation of motion for a pressure wave is given by [20]

$$\frac{\partial^2 \Delta\tilde{p}}{\partial t^2} - \Gamma'\nabla^2 \frac{\partial \Delta\tilde{p}}{\partial t} - \upsilon^2\nabla^2\Delta\tilde{p} = 0 \tag{2.1}$$

Here, $\tilde{P}$ is the pressure wave, t is time, υ denotes the velocity of sound, Γ' is the damping parameter and it can be expressed as [19]

$$\Gamma' = \frac{1}{\rho}\left[\frac{4}{3}\eta_s + \eta_b + \frac{\kappa}{C_p}(r-1)\right] \tag{2.2}$$

η_s and η_b are the shear viscosity coefficient and bulk viscosity coefficient

respectively. κ is the thermal conductivity, C_p is the compressibility and γ is known as the adiabatic index. The last term $\frac{\kappa}{C_p}(r-1)$ has much less contribution to Γ' compared with the first two terms. The propagation of the wave can be described as [19]

$$\Delta\tilde{p} = \Delta p e^{i(qz-\Omega t)} + c.c \tag{2.3}$$

Here, q is the propagating wave vector while Ω is the angular frequency of the acoustic wave. When (2.3) is substituted into equation (2.1), we get the relation between q and Ω as

$$\Omega^2 = q^2(\upsilon^2 - i\Omega\Gamma') \tag{2.4}$$

Then

$$q^2 = \frac{\Omega^2}{\upsilon^2}\left(\frac{1}{(1-i\Omega\Gamma'/\upsilon^2}\right) \tag{2.5}$$

Using the Maclaurin series expansion for the second term, we have

$$1+(i\Omega\Gamma'/\upsilon^2)+(i\Omega\Gamma'/\upsilon^2)^2+(i\Omega\Gamma'/\upsilon^2)^3+..... \tag{2.6}$$

If we just take the first two terms of (2.6) (as these two terms has the biggest contribution), then (2.5) can be written as

$$q^2 = \frac{\Omega^2}{\upsilon^2}(1+(i\Omega\Gamma'/\upsilon^2)) \tag{2.7}$$

Since

$$\sqrt{1+x} = 1+\frac{1}{2}x-\frac{1}{8}x^2+\frac{1}{16}x^3-.....+\frac{(-1)^n(2n)!}{(1-2n)(n!)^2(4^n)}x^n+..... \tag{2.8}$$

Using this relation for the second term of (2.7), still taking the first two terms q can be written as

$$q = \frac{\Omega}{\upsilon}+\frac{i(\Omega^2/\upsilon^2)\Gamma'}{2\upsilon} \tag{2.9}$$

Thus, the phonon decay rate is expressed as

$$\Gamma = \Gamma'\left(\Omega^2/\upsilon^2\right) \tag{2.10}$$

There are two components of the spontaneous Brillouin scattering: Stokes and anti-Stokes. The wave vector of the Stokes scattering is

$$\mathbf{k}' = \mathbf{k} - \mathbf{q} \tag{2.11}$$

k is the wave vector of input light and k' is the scattered wave vector. Its frequency is given by

$$\omega' = \omega - \Omega \tag{2.12}$$

ω is the input light's frequency while ω' is the scattered light's frequency. The dispersion relationships for the incident optical field, the acoustic wave, and the scattered optical wave are

$$\omega = |\mathbf{k}|c/n \tag{2.13}$$

$$\Omega = |\mathbf{q}|\upsilon \tag{2.14}$$

$$\omega' = |\mathbf{k}'|c/n \tag{2.15}$$

In order to make these relations to satisfy simultaneously, for any scattering direction the sound-wave frequency and wave vector should have particular values. If the scattering angle is θ as illustrated in fig 2.2.(a), as the absolute values of the incident wave vector and scattered wave vector are nearly equal, we have

$$|\mathbf{q}| = 2|\mathbf{k}|\sin(\theta/2) \tag{2.16}$$

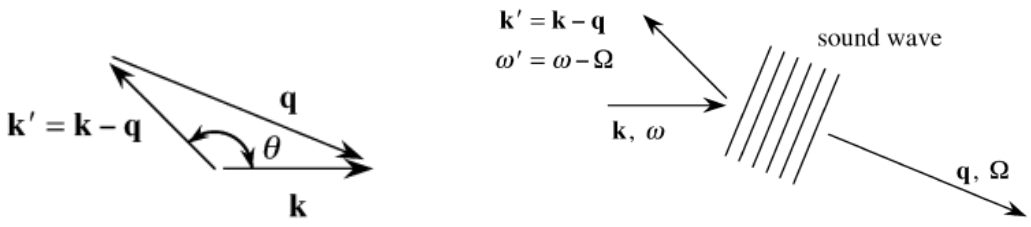

(a) (b)

Fig 2. 2. Diagrams of Stokes Brillouin scattering [19]

Subsequently, the frequency shift can be expressed as

$$\Omega = 2|\mathbf{k}|\upsilon \sin(\theta/2) = 2n\omega\frac{\upsilon}{c}\sin(\theta/2). \tag{2.17}$$

Thus, we can get the maximum Stokes shift which is given by

$$\Omega_{\max} = 2n\frac{\upsilon}{c}\omega \tag{2.18}$$

Stokes scattering can be regarded as the scattering of light from a retreating acoustic wave which is shown in fig 2.2.(b). For the anti-Stokes scattering which is illustrated in fig 2.3.(a), the analysis process is similar with the Stokes case.

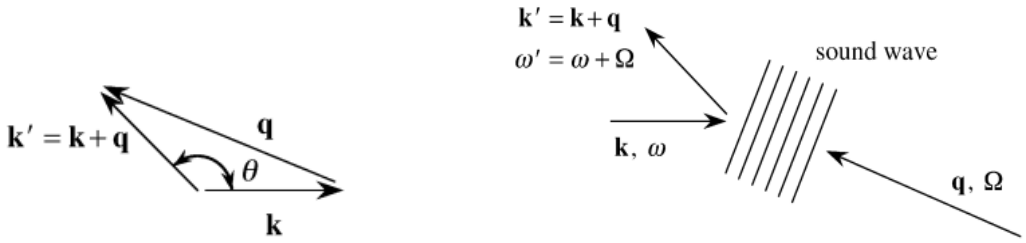

(a) (b)

Fig 2. 3. Diagrams of anti-Stokes Brillouin scattering [19]

The dispersion and frequency relationships should also be satisfied but with different signs as follows

$$\mathbf{k}' = \mathbf{k} + \mathbf{q} \tag{2.19}$$

$$\omega' = \omega + \Omega \tag{2.20}$$

The frequency shift is the same as in (2.18) when only the first order of the Brillouin frequency shift is considered. However, if the second order is also taken into account, the anti-Stokes Brillouin frequency shift is different from the Stokes Brillouin frequency shift [21]. The anti-Stokes scattering can be taken as scattering from an oncoming sound wave

which is shown in fig 2.4. (b).

If we consider the attenuation of the acoustic wave, the scattered light is not monochromatic but has a spread in angular frequency whose full width at half maximum (FWHM) is given by

$$\delta\omega = 1/\tau_p = \Gamma \tag{2.21}$$

Here τ_p is the lifetime of the acoustic phonon. Remembering (2.10), it can be inferred that the linewidth has squared frequency dependence on the pump light.

The stimulated scattering process occurs when the fluctuations are caused by the presence of the light field. This is different from spontaneous light-scattering process where the fluctuations are induced by thermal effects. For stimulated Brillouin scattering, the interference of the laser and Stokes fields has a frequency component which is equal to the frequency of the sound wave. In this way the amplitude of the sound wave is increased.

Consequently the Stokes wave is enhanced due to the beating of the laser wave with the sound wave. The beating of the laser wave and the Stokes waves will again reinforce the sound wave. This positive feedback will lead to the exponential growth of the amplitude of the Stokes wave. The mechanism of electrostriction which is the tendency of materials to become compressed in the presence of an electric field is commonly applied to explain the interference of laser and Stokes waves.

2.4 SBS Suppression

Stimulated Raman and Brillouin scattering will induce power dependent loss in optical fiber when the power densities are high [22] [23] [24]. This is caused by the severe attenuation of the forward traveling light as a result of the energy transferring to the stimulated backward wave. The maximum achievable optical power of a fiber is determined by stimulated Brillouin scattering [25] which normally has a lower threshold than other nonlinear effects [9]. In the applications where high optical power is required such as nonlinear devices, fiber amplifiers and lasers, fiber to the home etc, there is an increasing interest in reducing the SBS effect [10] [11] [12] [26] [27].

When the laser's linewidth is much larger than the Brillouin linewidth, SBS can be effectively suppressed [28]. Therefore, broadening the laser spectrum becomes the simplest way to suppress SBS [29] [30] [31]. However, when a narrow linewidth signal is required for a fiber laser or amplifier, this method cannot be adopted. Other techniques like inducing stresses in the fiber [32], varying the index of refraction [33] and varying core size in an acoustic guiding fiber [34] were proposed. However, to obtain large SBS suppression, these methods are both difficult and expensive to implement. Recently, a fiber structure with tailored acoustic-wave guiding properties is examined experimentally for SBS suppression [28]. In this structure, the optical core is surrounded by a highly multimode acoustic waveguide. As a result, the Brillouin scattering bandwidth is broadened and the Brillouin gain coefficient is reduced. The advantage of this design is that the optical guiding properties of the central core are not affected and the fiber

structure remains uniform. Thus, this becomes a practical way for SBS suppression.

2.5 Conclusion

Different optical fibers have their own advantages and disadvantages. How to choose the right fiber for a special function is very critical. The standard SMF is traditionally used for the purpose of sensing while the dispersion shifted fiber (e.g. LEAF), which has a comparable price and advantages, is worthwhile to be investigated for Brillouin temperature and strain sensing. From the derivation of the linewidth in the spontaneous Brillouin scattering, the Brillouin linewidth is squared frequency dependent on the pump light. However, this is just a theoretically estimated result and probably can be only held for the step-index fiber. Much deeper research into the linewidth's wavelength dependence of complex structured index profile fiber needs to be done. This study can be beneficial to the SBS suppression where the optical fibers with modified acoustic waveguide structures are widely used.

Chapter 3

Verification of Frequency Square Law for Intrinsic Brillouin Linewidth in LEAF fiber

Study at the wavelength windows of 1.3μm and 1.55μm for the wavelength dependence of Brillouin spectral width provides useful information for stimulated Brillouin scattering (SBS) suppression in SMF. A frequency square law is traditionally used to describe the spectral width's dependence on light wavelength theoretically based on a damped oscillator model, which is valid for bulk material. With complex structured waveguide of SMF to suppress SBS, it is important to verify the widely used model by measuring the Brillouin spectral width of LEAF. We found that the third and fourth peaks of LEAF don't satisfy the frequency square law when the waveguide structure has a major contribution to the linewidth.

3.1 Introduction

In lightwave transmission systems, precise measurements of Brillouin gain spectra are of great importance [35] [36] [37]. The SBS can be a major limit when high power is transmitted in single mode fiber. Thus, high SBS threshold is required. One of the methods to suppress SBS is to manipulate the sound velocity profile by refractive index

change in the core and cladding region [10] [38] [39]. When the Brillouin gain coefficient of a certain strength is required, the Brillouin spectral width is one of the important parameters that need to be designed. For a specific system or application, this value can be maximized or minimized. Since LEAF fiber has a triangle refractive index profile at the core area, it is necessary to study the Brillouin linewidth's frequency dependence in this fiber.

3.2 Brillouin Linewidth

The changes in the dielectric constant resulting from density fluctuations lead to the scattering of light by condensed matter. Temperature or pressure fluctuations will cause the local changes in density. The density fluctuations due to temperature cannot propagate. It will decay owing to a large thermal conductivity. Rayleigh scattering is affected by this mechanism. The fluctuations due to pressure can propagate with the velocity of sound v. This leads to Brillouin scattering [40].

The density fluctuations will dissipate as time progresses. Those caused by pressure changes attenuate because of friction. All phenomena which cause an irreversible generation of heat from mechanical energy are referred to as "internal friction". The observed internal friction effect (the energy absorption) in fused silica appears to result from structural relaxation [41]. The energy dispersion involved in this process is represented in a broadening of the peaks in the Brillouin spectrum [42]. A frequency square law of the Brillouin linewidth is expected theoretically [19] [43]. Since the

Brillouin frequency shift (V_B) varies inversely with the pump wavelength, the Brillouin linewidth is also expected to obey a λ_p^{-2} dependence on the pump wavelength.

3.3 Historic Experimental Results

The experiment of the ultrasonic attenuation in fused silica using Bragg diffraction of light is performed [44]. For longitudinal and transverse modes, the frequency dependence of the attenuation over the frequency range of 200-980MHz is given by $f^{1.97}$ and $f^{1.98}$ respectively. This result is consistent with the square-law frequency dependence. Then the Brillouin-gain spectra were measured for a G_eO_2-doped core/fused-silica cladding and a fused-silica core/F-doped cladding fiber respectively [45]. It was found that the intrinsic Brillouin linewidth varies with λ^{-2} for these two kinds of fibers.

However, it was reported that the fibers containing boric oxide do not follow the conventional frequency squared law [46]. It mentioned that in the expression for the Brillouin spectral width the dynamic viscosity term is frequency dependent. It was shown that when the temperature of the peak of the viscosity curve at hypersonic frequencies lied far from a fiber's fictive temperature, the linewidth obtained a simple frequency-squared dependence. And this was just the case for SMF-28^{TM} as they demonstrated. As for the boric doped fiber, the peak of viscosity lied in the vicinity of a fiber's fictive temperature. Therefore, a departure from the rule is expected. This analysis removed the uncertainty in the measurements caused by non-uniform acoustic profiles by

considering only the fundamental acoustic mode which was well-confined to the uniform region of the fiber [46]. Therefore the waveguide structure's influence was neglected.

In our research, this waveguide structure's influence is considered. After studying the four peaks of LEAF fiber, we found that the third and fourth peaks' linewidth ratio didn't follow the frequency square law. This means the waveguide structure also makes some contributions to the linewidth. The coupling effects between different peaks lead to the different reactions of the four peaks of LEAF. As a matter of fact, the frequency squared law is deduced in the fused silica where the material damping is the sole contributor. For comparison, we also tried the same experiment on SMF-28^{TM}. This kind of fiber satisfies the frequency square law as expected [46].

3.4 Experimental Setup

The experimental setup is shown in figure 3.1. The frequency counter is used to lock the frequency difference between the two lasers. After passing through the adjustable attenuator and a 95:5 coupler, the power from laser 1 is directed into the circulator. Propagating in the 21km LEAF fiber under test, the Brillouin back scattered light is produced which includes both the Stokes and anti-Stokes components. Then, it is combined with 99% of the power of laser 2 for heterodyne coherent detection [47]. As the closer the two signal's frequency is, the more likely beat signal can be produced. Therefore, when the frequency of laser 1 is higher than that of laser 2 the Stokes

component can be detected while the anti-Stokes component can be acquired when the frequency of laser 1 is lower than that of laser 2.

By adjusting the frequency difference between laser 1 and laser 2, we can shift the back scattered light into any frequency range we want. For example, the frequency shift of the first peak for the 1319 nm laser case is about 12530 MHz. Then we can tune the frequency difference between the two lasers to be 12400 MHz. In this way, the detected signal's first central frequency is altered to the lower frequency of about 130 MHz. Therefore, a lower bandwidth detector, in our case 1GHz, can be used to detect the signal. And the signal to noise ratio is also improved owing to the heterodyne coherent detection.

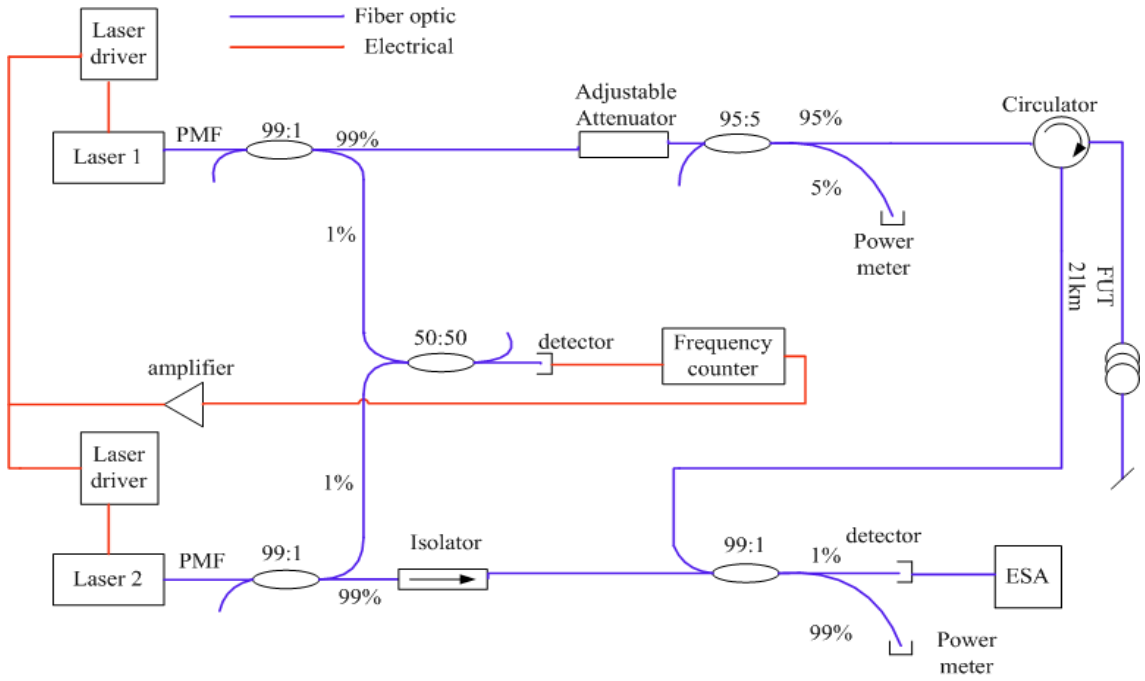

Fig 3. 1. System setup for 1319 nm laser input.

The 1550nm system setup is almost the same as 1319nm case. The difference are: (1) a variable attenuator is applied after the isolator and (2) the second coupler at the bottom

is changed from 99:1 to 50:50 since the input power of one of the lasers is only 16mW. In the 1319nm case the laser output is 110mW. Employing the 50:50 coupler ratio can maximize the coupling efficiency of signal and the local oscillator without saturating the detector. It has a maximum 1mW power input to work in the linear region.

3.5 Experimental Result-Stokes

It was shown that the linewidth of the four peaks for LEAF would decrease when the input power was increased to some value [48]. As a result, we chose the relatively low input power to measure the linewidth before it starts to decrease. Figure 3.2 illustrates the measured spectrum for both the 1550 nm and 1319 nm cases of the Stokes component. When the laser has a wavelength of 1550 nm, the input power at the circulator is 351 μW while for the 1319 nm case, this value is 367.9 μW.

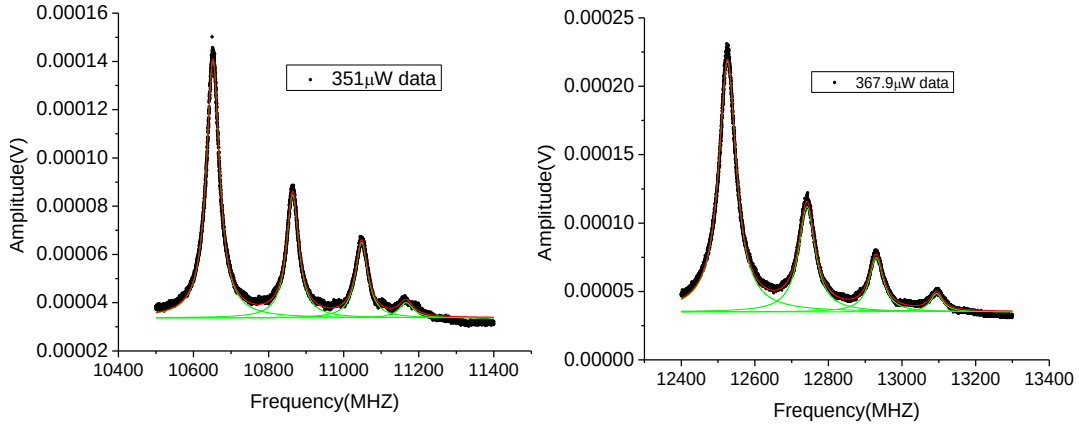

(a) (b)

Fig 3. 2. (a) and (b) are the measured spectrums for 1550nm and 1319nm cases of LEAF fiber for the Stokes component respectively.

We applied the Lorentz multi-peak curve fit to the original data. The fitted values for the linewidth, Brillouin peak frequencies and relative peak power (RPP) are listed in table 3.1. The two lasers we used have KHz range linewidth. So the fitted linewidth is just the intrinsic value. Since the square of the two laser's wavelength ratio is 1.38, we can see that the linewidth ratios for the last two peaks are less than this number. This means that the frequency squared law is no longer correct when the waveguide structure starts to play an important role. The uncertainties for the linewidth in the 1319 nm wavelength are 0.08, 0.19, 0.35 and 0.97MHz from peak 1 to peak 4. The uncertainties for the linewidth in the 1550 nm wavelength are 0.07, 0.15, 0.25 and 1.37MHz from peak 1 to peak 4.

Table 3. 1: Measured spectral characteristics of LEAF fiber in the spontaneous regime for the Stokes component.

	1319nm			1550nm			Ratio
	$\triangle V_B$(MHz)	V_B(MHz)	RPP	$\triangle V_B$(MHz)	V_B(MHz)	RPP	$\triangle \mathbf{V_B}^{1319} / \triangle \mathbf{V_B}^{1550}$
PEAK 1	57.22	12526	1.00	42.21	10651	1.00	1.35
PEAK 2	54.97	12741	0.51	39.86	10864	0.60	1.38
PEAK 3	47.19	12929	0.34	40.11	11048	0.46	1.18
PEAK 4	40.64	13094	0.22	45.68	11166	0.28	0.89

The different linewidth ratios for the four peaks of LEAF fiber are attributed to the coupling effects among each other. Take the wavelength of 1319nm for example, for peak 1 and peak 2, due to the large frequency separation (215MHz) and large peak power difference (50%) the coupling effect between them is very small. Since the peak power of peak 3 is reduced further to only 34% of peak 1. Peak 3 has little impact on peak 2. Therefore, peak 2 has the linewidth ratio value closest to 1.40. As the peak power of peak 4 is only 22% of peak 1, peak 1 and peak 2 have much greater impact in peak 3. As a

result, peak 3 has a linewidth ratio of 1.18 which doesn't satisfy the frequency square law. Peak 4 has the lowest peak power and the first three peaks' contribution made its linewidth ratio reduced further to 0.89.

For comparison, we also measured the linewidth of 25km of SMF-28^{TM} for the two wavelengths. The input powers for the 1319nm and 1550nm lasers are 367μW and 340μW respectively. The measured spectrums are shown in figure 3.3. The higher order acoustic modes are visible.

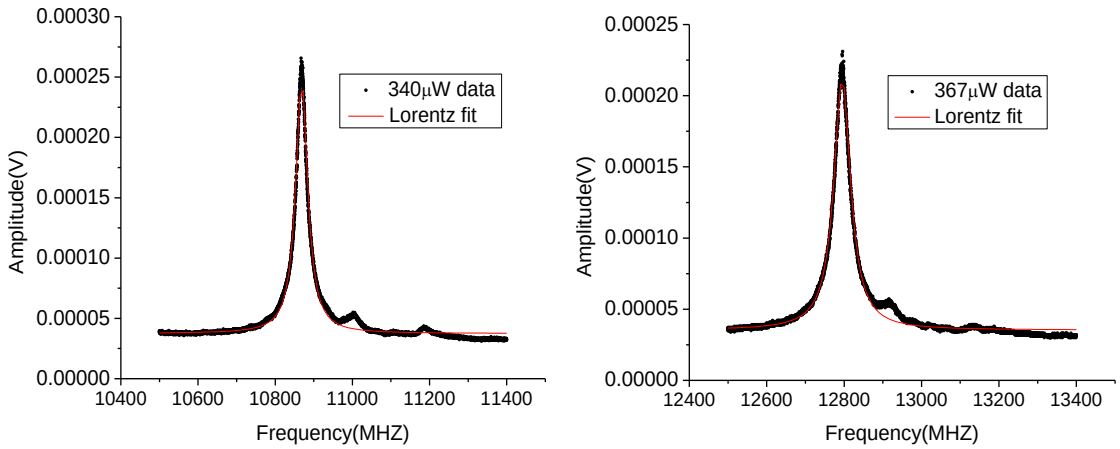

(a) (b)

Fig 3. 3. (a) and (b) are the spectrums of the 1550nm and 1319nm cases of SMF for Stokes scattering .

Table 3.2 shows the spectrum characteristic of SMF-28^{TM}. Since the linewidth ratio for the two wavelengths is 1.40, it can be inferred that SMF-28^{TM} follows the frequency square law in the Stokes case.

Table 3. 2: Linewidth and Brillouin central frequencies of SMF-28^{TM}

	$\triangle V_B$(MHz)	**Linewidth uncertainty**	**V_B(MHz)**

		(MHz)	
1319nm	52.02	0.11	12795
1550nm	36.96	0.08	10868
Ratio ($\triangle V_B^{1319}/\triangle V_B^{1550}$)	1.40		

For LEAF fiber, the dispersion at 1550nm is about 4 ps/nm-km while at 1319nm this value is -22 ps/nm-km. The waveguide contribution is much larger in LEAF fiber than in SMF. The fiber non-uniformity which is induced by manufacturing process and the complex index profile caused the variations of the optical and acoustic waveguide. If we look at the four peaks' ratio of LEAF fiber, they are all different from each other. This confirms that the wave guide structure will influence the frequency square law.

3.6 Experimental Result-Anti-Stokes

Since the Stokes component involves phonon creation while the anti-stokes component is accompanied by phonon annihilation, their linewidths' frequency dependence may have different behavior. Therefore, we also measured the linewidth of LEAF and SMF-28^{TM} for the anti-Stokes component in 1319nm and 1550nm wavelengths in fig 3.4.

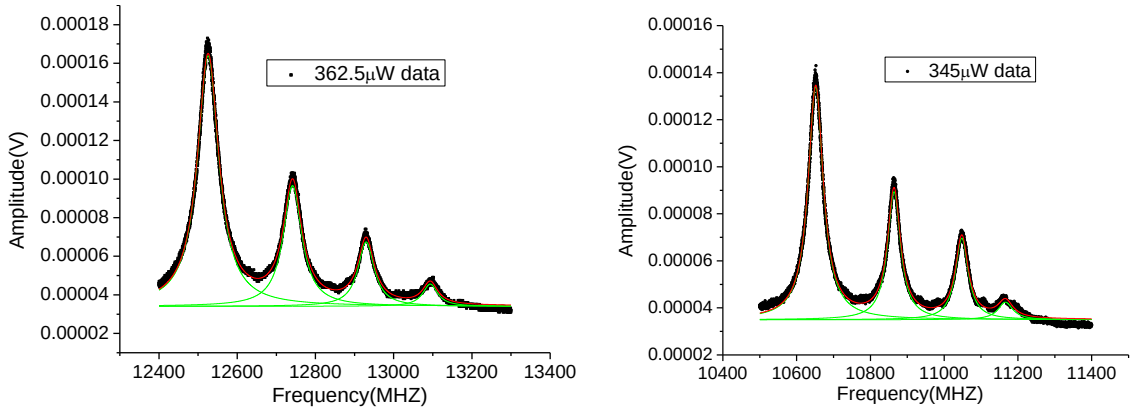

(a) (b)

Fig 3. 4. (a) and (b) are the measured spectrums for 1319nm and 1550nm cases of LEAF fiber for the anti-Stokes component respectively.

Using the Lorentz curve fit in both of the two wavelengths range, we obtained the linewidths for the four peaks of LEAF fiber in table 3.3. It is shown that the first two peaks satisfy the frequency square law as the linewidth ratios are very close to 1.38. For the last two peaks, the ratios have much smaller value than 1.38. Thus, they don't satisfy the frequency square law. This tendency is the same as in the Stokes case. However, the ratios in the anti-Stokes case are smaller than in the Stokes case for the first two peaks, while for the last two peaks they are larger than in the Stokes case. It is also noted that the linewidths in the anti-Stokes case is larger than in the Stokes case. The frequency separation between different peaks is the same as in the Stokes case while the RPP from peak 2 to peak 4 are larger in the anti-Stokes case comparing to the Stokes case. Therefore, the coupling effect between peak 1 and peak 2 is larger. This caused a smaller linewidth ratio of peak 1. With a stronger impact induced by peak 3, peak 2 also has a smaller linewidth ratio. Owing to the larger effect from peak 1 and peak 2 than peak 4, peak 3 has larger value of the linewidth ratio. At the same time peak 4 also has a larger linewidth ratio due to the larger coupling effect from the first three peaks.

The uncertainties for the linewidth in the 1319 nm wavelength are 0.09, 0.18, 0.31 and 0.90 MHz from peak 1 to peak 4. The uncertainties for the linewidth in the 1550 nm wavelength are 0.1, 0.17, 0.26 and 1.37 MHz from peak 1 to peak 4.

Table 3. 3: Measured spectral characteristics of LEAF fiber in the spontaneous regime for the anti-Stokes component.

	1319nm			1550nm			Ratio
	$\triangle V_B$(MHZ)	V_B(MHZ)	RPP	$\triangle V_B$(MHZ)	V_B(MHZ)	RPP	$\triangle \mathbf{V_B}^{1319}/ \triangle \mathbf{V_B}^{1550}$
PEAK 1	66	12526	1.00	49.6	10651	1.00	1.33
PEAK 2	57.6	12741	0.60	42.76	10864	0.66	1.35
PEAK 3	50.24	12929	0.42	41.97	11047	0.52	1.20
PEAK 4	46.31	13093	0.28	48.68	11166	0.31	0.95

Since the wavelengths used are far from the zero-dispersion wavelength of LEAF fiber which makes the phase matching condition required for four-wave mixing unsatisfied, it is inferred that the anti-stokes Brillouin scattering is caused by phonon annihilation instead of four wave mixing [49]. In this case, both the Stokes and anti-Stokes Brillouin scattering are generated by thermally excited acoustic waves which are distributed in the fiber. However, the difference is that the phonon annihilation in the anti-Stokes case will lead to the decrease of the acoustic phonons. As a result, the anti-Stokes waves are subjected to attenuation owing to the energy transfer to the input laser light [49]. This has lead to the different behaviour of LEAF fiber in the Stokes and anti-Stokes cases.

Using the same method, we also measured the linewidth of SMF-28^{TM} for different wavelengths which is shown in fig 3.5.

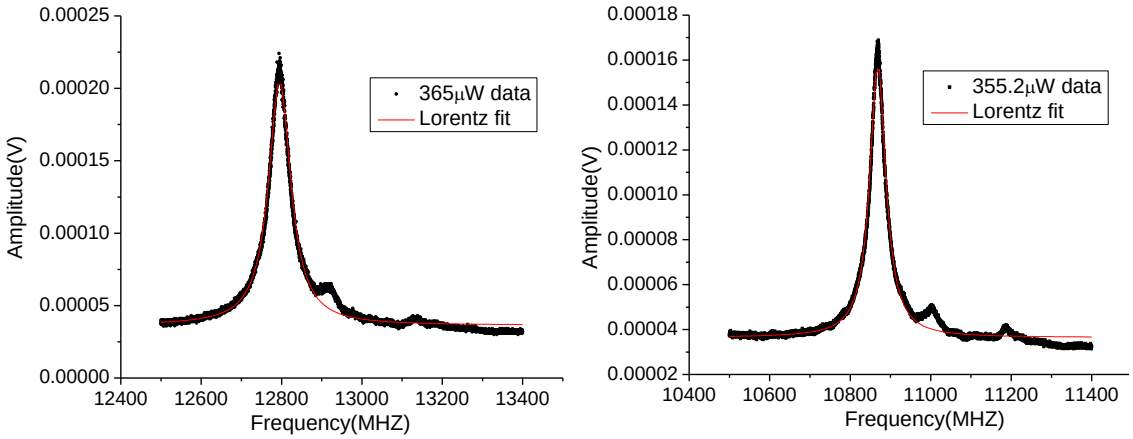

(a) (b)

Fig 3. 5. (a) and (b) are the spectrums of the 1319nm and 1550nm cases for SMF-28^{TM} in the anti-Stokes case.

The result of the linewidth and the ratio for two different wavelengths is shown in table 3.4. We found that the linewidth ratio is the same as in the Stokes case. This means that the frequency square law can be held in both the Stokes and anti-Stokes cases for the SMF-28^{TM}. Since the 1st peak dominates the Brillouin gain spectrum the coupling effect from 2nd peak is negligible, hence the single oscillator model of frequency square law holds well as it is close to the bulk material case. Here, waveguide structures have little contribution to the spectral linewidth via multiple peaks coupling effect.

Table 3. 4: Linewidth and Brillouin central frequencies of SMF-28^{TM} in the anti-Stokes case

	$\triangle V_B$(MHZ)	**Linewidth uncertainty (MHZ)**	**V_B(MHZ)**
1319nm	66.29	0.17	12795
1550nm	47.34	0.12	10868
Ratio ($\triangle V_B^{1319}$/ $\triangle V_B^{1550}$)	1.40		

The experiments were repeated for five times. For each of the time, the uncertainty

of the linewidth was obtained by fitting the spectrum with Lorentz curve. The overall uncertainty was calculated by averaging the five uncertainties. The experimental data points were attained every 0.1125MHz by ESA.

3.7 Discussion

If we look at equation (2.1), when there were several acoustic modes guided in the fiber, the sound velocities for different acoustic modes would be different. They should have their own equations of motion for the pressure waves. Therefore, the linewidths which is illustrated in (2.10) are different for all the acoustic modes, and all of them contribute to the Brillouin gain. Hence there is acoustic-optical coupling effect via Brillouin gain. The spectral distribution of Brillouin light scattering can be found in [50], and the waveguide theory of acoustic modes are demonstrated in [51].

Instead of the optical effective area which was conventionally used to describe SBS in optical fiber, the acousto-optic effective area was introduced [1]. And this term represents for the waveguide structure's influence. The Brillouin linewidth corresponding to different acoustic modes was given in (A.31) [1]. This is why the third and fourth peaks of LEAF fiber don't satisfy the frequency square law, as peak 3 and 4 present strong coupling of different peaks which is not being considered in the calculation of frequency square law relation. The profiles of acoustic modes and acousto-optic effective areas for standard single mode fiber and LEAF fiber are calculated in table 2 [1]. We can see that the acousto-optic effective areas of the 2nd and 3rd acoustic modes for LEAF

fiber are 274.8μm^2 and 842μm^2 compared with those of SMF which are 3928μm^2 and 4921μm^2 respectively. This means the 2nd and 3rd acoustic modes of LEAF fiber has a stronger overlap with the optical mode than those of SMF fiber [10]. Since the frequency squared law is deduced with one damped oscillator model [19], when there are several acoustic modes having strong waveguide features this rule may not be able to describe correctly the whole process.

Therefore, the frequency squared law which was deduced in fused silica cannot be used to describe the linewidth wavelength dependence ratio when the waveguide structure begins to play an important role. From our experimental results, it is obvious that a modified model should be introduced to describe the frequency dependence of the linewidth in optical fiber for the complex index profile fibers, such as LEAF fiber.

3.8 Conclusion

We performed the spontaneous Brillouin scattering experiment in 1319nm and 1550nm wavelengths for both LEAF and SMF-28^{TM} fibers. The results showed that the Brillouin linewidth of SMF-28^{TM} satisfied the frequency squared law in both the Stokes and anti-Stokes cases while the third and fourth peaks of LEAF fibers don't have this feature. After all, the theoretical model was derived in fused silica. Since the waveguide contribution also influence the measured spectral width, the frequency squared law may not be correct in fiber where there are higher order acoustic modes that are overlapping with the optical mode. Therefore, a more complete model is needed to describe the

frequency dependence of the spectral width for Brillouin scattering in the optical fiber.

Chapter 4

Brillouin Spectrum in LEAF and Simultaneous Temperature and Strain Measurement

The triangle refractive index profile of LEAF fiber (a non-zero dispersion shifted fiber) makes it much more sensitive to temperature and strain. Owing to its high stimulated Brillouin scattering (SBS) threshold for long distance distributed sensors, we studied the Brillouin spectrum characteristics of LEAF under different strain and temperature conditions. The results are compared with those of SMF-28. Based on the linear relationship between the four peaks' linewidth/peak frequency and strain/temperature, we achieved a strain error of 37με and a temperature error of 1.8°C with a spatial resolution of 4 m for simultaneous temperature and strain measurement.

4.1 Simultaneous Temperature and Strain Measurement

For distributed sensing based on SBS, the problem of cross sensitivity where the Brillouin frequency is sensitive to both temperature and strain makes the change in temperature and strain indistinguishable [52][53]. The effects of temperature may be negligible in the laboratory conditions where the temperature variation is very small. However, in the field applications as the temperature variations from one location to

another in a large structure can be very different, simply ignoring the temperature effect may bring many measurement errors [54], especially for the field condition that the structure is subjected to small strains (< 100με) [55].

The earliest solution to this problem was arranging an optical fiber such that it passed through the same path twice while one of the paths was isolated from strain [56]. And this path could be applied to detect the Brillouin frequency shift produced by temperature. Then the frequency shift induced by strain of the other section could be recovered by subtracting the combined frequency shift from that originated from temperature effects. They achieved a 22-km sensing length, a strain resolution of 20με and a temperature resolution of 2 ℃ with a spatial resolution of 5 m.

In order to use only one fiber section, it was reported that by measuring the power and frequency shift of noise-initiated Brillouin scattering, the strain and temperature effects could be resolved [57]. By mathematically combing the values of the Stokes and anti-Stokes powers to produce a linear effective power and using backscattered Rayleigh signal as a reference, the preliminary results arrived at a strain resolution of 100με strain, a temperature resolution of 4 ℃ and a spatial resolution of 40m, over a sensing length of 1200m in SMF-28 [58]. Here, the spatial resolution is restricted by the relatively low signal levels. Thus this technique is not suitable for many practical strain-sensing applications. Using the same principle, the system was improved by using cascaded Mach-Zehnder interferometric filters [59]. A temperature resolution of 4 ℃, a strain resolution of 290με and a spatial resolution of 10m for a sensing length of 15 km were attained [59]. However, the spatial resolution is still not good enough due to weak

spontaneous Brillouin scattering.

By incorporation of the Brillouin loss peak power with the conventional Brillouin-frequency measurement (which is a SBS process), a strain and temperature resolutions of ±178με and ±3.9 ℃ at a spatial resolution of 3.5m were obtained with 50m sensing fiber [54]. This Brillouin-loss mechanism provided much better signal levels than the former method. Hence, the spatial resolution was improved by more than ten times. The measurement error induced by polarization drifting has been reduced by the PM fiber. However, the polarization alignment of this fiber is much more difficult to handle.

Recently multi-peak Brillouin spectrum was explored for the discrimination due to the different dependence of each peaks' V_B on temperature and strain. The first and second Brillouin peaks of the LEAF fiber were applied to achieve a temperature resolution of 5°C, a strain resolution of 60με and a spatial resolution of 2m over a 3682m sensing length [60]. It is a very elegant and exciting approach, but the sensing fiber length is only 3.7km. Soon afterwards the fiber length was extended to over 22km [61]. The temperature and strain errors were calculated to be 27°C and 570με respectively. Comparing to the SMF-28 which were 4.10 ℃ and 140με correspondingly [61], the two frequency components of LEAF produced much larger measurement errors. For temperature information, the differential frequency change of the first two peaks was about 190 kHz/ ℃ comparing with SMF's 1MHz/ ℃. This put a very high requirement on the frequency resolution. Since they used the BOTDR system, kHz range frequency resolution was very hard to attain due to the weak Stokes signal.

Shortly after that, the first and third peaks' central frequency of the photonics crystal fiber were utilized to reach a temperature and strain error of 3.9°C and 83με with the spatial resolution of 15cm. The sensing length is 2m [62]. This result showed much higher measurement accuracy than in LEAF fiber, and it was attributed to the higher power density for a small core of the PCF. Combining this with the BOTDA system resulted in higher Brillouin gain-loss and a better SNR. However, the problem is that the presence of multiple sub-peaks with close frequency spacing in the Brillouin gain spectrum (BGS) makes them hard to separate. Then the simultaneously strain and temperature measurements with PMF were investigated [63]. The Brillouin frequency, peak power and bandwidth were all used for the error analysis, however, the temperature and strain resolution were not improved much.

Recently Zou *et al.* applied the four peaks' central frequency of a high-delta fiber with F-doped depressed inner-cladding to solve the problem and they got the temperature and strain error of 1.8°C and 44με with the sensing length of 4.74m [64]. Since all the peak frequencies had similar dependences on temperature and strain (V_B increases with both temperature and strain), accurate discrimination still couldn't be realized. Then a novel method was raised using one piece of panda-type polarization-maintaining fiber. They demonstrated that V_B and the birefringence-determined frequency deviation in this PMF had the same signs of strain dependence but the opposite signs of temperature dependence. This made the temperature and strain much easier to discriminate. And they realized an accuracy of 3με and 0.08°C in 31m long fiber using CW waves. A distributed discrimination of temperature and strain was then demonstrated with 10-20cm spatial

resolution [65] [66]. This method uses the Brillouin grating to measure the birefringence and Brillouin frequency change, which makes the measurement system complicated [67], and with PMF the launching of fiber axis is complicated.

In order to use a relatively simpler experimental set-up and obtain high accuracy, we used the BOTDA system [55] making LEAF as the sensing fiber. Although the first two peaks' V_B have been explored for the temperature and strain discrimination, we studied the linewidth and peak power of the four peaks of LEAF fiber for their temperature and strain dependence and also explored the discrimination of temperature and strain for the first time. We found that the four peaks' linewidth were decreasing with increasing temperature or strain which was opposite to the behavior of Brillouin central frequency shift. However, the peak power was not linearly related with temperature in a large range from 0^{o} C to 80^{o} C which made it unsuitable for the discrimination. Applying each peak's linewidth and V_B for the discrimination, we arrived at a strain error of 37με, temperature error of 1.8 ℃ and a spatial resolution of 4m.

4.2 Theory

SMF 28 is commonly used in long distance optical communication systems. This type of fiber normally has a 9-μm core diameter and a 125-μm cladding diameter with a simple step-index structure. It has a zero-dispersion at 1310nm wavelength while the dispersion value at 1550nm is about 17ps/nm-km [47]. The relatively high chromatic dispersion around 1550 nm induces significant waveform distortion at high speed (>

10Gb/s) fiber communication systems.

The NZDSF were introduced to reduce CD and the nonlinear crosstalk at 1550nm. For this kind of fiber, the CD around 1550nm is smaller than SMF but larger than DSF. LEAF is one example of this fiber. Its CD around 1550nm is about 4ps/nm-km while at 1310nm the value is about -15ps/nm-km.

The group velocity dispersion (GVD) has two components: material dispersion and waveguide dispersion which can be expressed as [68]

$$D_M = -\frac{2\pi}{\lambda^2}\frac{dn_{2g}}{d\omega} = \frac{1}{c}\frac{dn_{2g}}{d\lambda} \tag{4.1}$$

$$D_W = -\frac{2\pi\Delta}{\lambda^2}\left[\frac{n_{2g}^2}{n_2\omega}\frac{Vd^2(Vb)}{dV^2} + \frac{dn_{2g}}{d\omega}\frac{d(Vb)}{dV}\right] \tag{4.2}$$

Here n_{2g} is the group index of the cladding material and the parameter V and b are given by [68]

$$V = k_0 a(n_1^2 - n_2^2)^{1/2} \tag{4.3}$$

$$b = \frac{\beta/k_0 - n_2}{n_1 - n_2} = \frac{\bar{n} - n_2}{n_1 - n_2} \tag{4.4}$$

n_1 and n_2 are refractive index of fiber core and cladding while $\bar{n}$ is the mode index or effective index and Δ is the index step, a is the core radius and k_0 is the free-space wave number. The V parameter plays an important role in determining the cutoff condition.

There are different kinds of SMF such as SMF-28e (step index), LEAF (triangle index) and SMF-28e+ (double cladding). SMF-28e has one Brillouin peak while SMF-28e+ has two Brillouin peaks [69], and LEAF has four Brillouin peaks, which is chosen for our experimental work. The smaller CD of LEAF at 1310nm represents that the waveguide contribution dominates the dispersion [68], which in turn governs

temperature and strain dependence for birefringence part, i.e. n dependence on V_B and gain. Besides, the multi-Brillouin peaks of LEAF fiber means smaller SBS gain. This induces smaller pump depletion and higher SNR, which are very important for long distance (> 60km) distributed sensors [70].

4.3 Experimental Set-up and Results

4.3.1 Experimental Set-up

The distributed Brillouin sensor used is a BOTDA system based on two 1319nm Nd: YAG lasers which are probe and pump sources respectively. The experimental set up is illustrated in Fig 4.1.

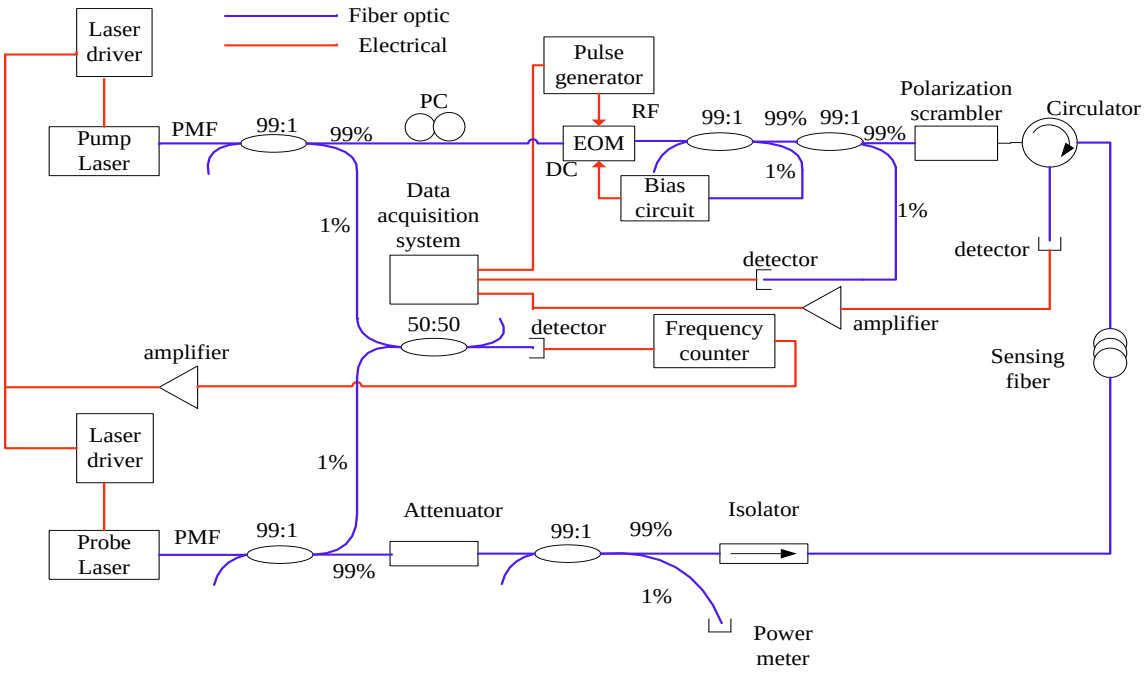

Fig 4. 1. Experimental set up based on BOTDA.

Light from the pump laser first passes a section of PMF which is the tail fiber of the laser and then go through a 99:1 coupler where 99% of the power is transmitted to an electro-optic modulator (EOM). Before the EOM there is a polarization controller to adjust the polarization state of the light. The EOM will be controlled by a pulse generator and a Bias circuit where the RF and DC will be adjusted. Once passed through the EOM the initial CW light will become a pump pulse. After the two 99:1 couplers, 1% of the power will be sent to the detector to detect the power of the pump pulse. Following up is a polarization scrambler which is applied to continuously change the polarization state of the pump pulse so that the polarization's effect (the signal fluctuation induced by polarization mismatch between pump and probe) can be minimized. Then the pump pulse will enter the circulator and interact with the counter propagating CW probe in the sensing fiber.

The light coming from the probe laser will also first pass a section of PMF and then be split by a 99:1 coupler where 1% of the power will be combined with 1% of the power from the pump laser to control the frequency difference between pump and probe lasers by the frequency counter. The rest of the 99% power will first enter an attenuator to control the power lever of the probe laser so as not to saturate the detector following the circulator. After the attenuator a 99:1 coupler will split 1% of the power into the power meter to monitor the power, then 99% of the power will go through an isolator and this will help to protect the probe laser source from the reflected light. By passing through the sensing fiber the probe signal is amplified and will be detected by an AC detector. This signal will then be received by the data acquisition system where analysis of the signal is

performed.

The monitored pump power and probe power are 35.4mw and 500μw respectively. The pulse width we used is 40ns. Since the spatial resolution is determined by (cW)/ (2n) where c is the speed of light in vacuum, W is the pulse width, and n is the refractive index of the fiber core. Therefore, in our experiment, a spatial resolution of 4m is expected. In the strain experiment the fiber section under strain is a 4.24m LEAF fiber and the total sensing length is 112m. We used the translation stage with micrometer to change the strain experienced by the fiber and also to read the length change from the micrometer. The length of the LEAF fiber was strained eight times with 4mm change each time which corresponded to 943.4με. As the system error for the translation stage is 0.01mm, the strain error is (943.4 με/4 mm) ×0.01 mm=2.3με. In the temperature experiment the fiber in the oven is 90m LEAF fiber and the total sensing length is 377m. The temperature was changed from 0℃ to 80℃ in increments of 10℃. As we read the temperature from the thermometer, the temperature error is 0.1℃. Since there will be more low frequency information in the signal when the fiber is longer [71], we used a 100Hz-350MHz AC detector in the temperature experiment instead of the 1GHz AC detector with an electrical amplifier used in the strain experiment. Consequently the power reading appears much smaller in the temperature situation.

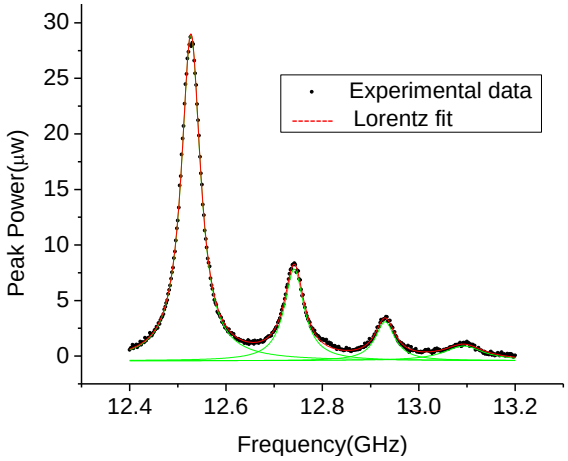

Fig 4. 2. Lorentz curve fitting of LEAF fiber's BGS at loose strain and room temperature.

From Fig 4.2 we can see that the Brillouin gain spectrum of the LEAF fiber can be fitted fairly well with Lorentz curve.

4.3.2 Strain Experiment

When the fiber is under strain, the volume of the whole fiber will change and this directly leads to the density change which is expressed as [72]

$$\rho = \rho_0 \frac{V_0}{V} = \frac{\rho_0}{(1+\varepsilon)(1-p_r\varepsilon)^2} \tag{4.5}$$

Due to the photoelastic effect, the refractive index is also dependant on strain. In an optical fiber the refractive index change is [73]

$$\Delta n = -\frac{n_0^3}{2} p\varepsilon \tag{4.6}$$

The V_B change results from the variation of the refractive index and the acoustic velocity upon strain. The acoustic velocity has the following form [74]

$$V_A = \sqrt{\frac{E_C(1-p_r)}{(1+p_r)(1-2p_r)\rho}} \tag{4.7}$$

E_C and p_r are the Young's Modulus and Poisson's ratio. The Young's Modulus has a slight dependence on the strain. With both the change of Young's Modulus and the density the acoustic velocity will change.

It is observed that there is a negative dependence of the Brillouin peak power on strain for SMF-28 [75]. This dependence is attributed to the dependence of the Brillouin gain's peak value on the strain. And it is given as [9]

$$g_{B0} = \frac{4\pi n^7 p^2}{3c\lambda^2 \rho V_A \Delta\nu_B} \tag{4.8}$$

p represents the longitudinal photoelastic coefficient. When the expressions of refractive index, density and acoustic velocity are all substituted into this equation, a negative dependence of the gain on strain will be expected. Owing to this effect, it was found that the Brillouin peak power was linearly related with strain [72].

Using the Lorentz curve fitting for the Brillouin gain spectrum the peak power change of the four peaks under different strain situations was measured (Fig 4.3.).

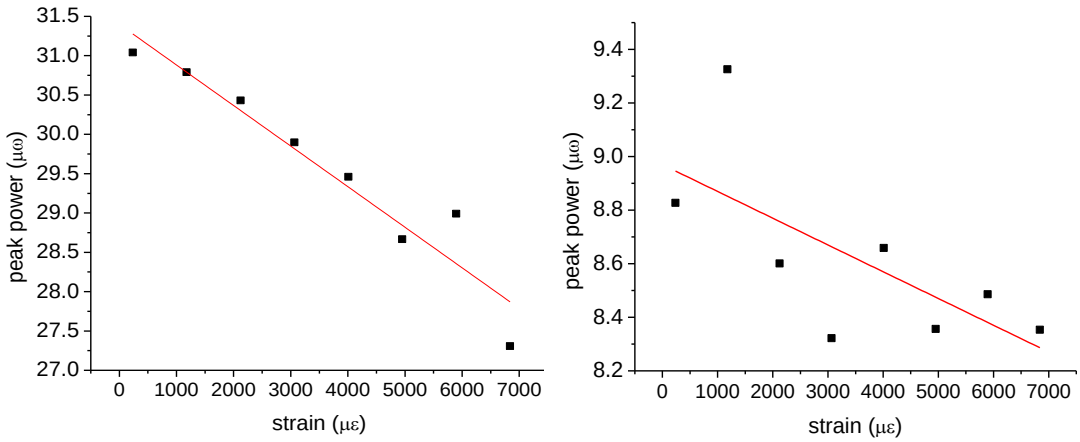

(a) (b)

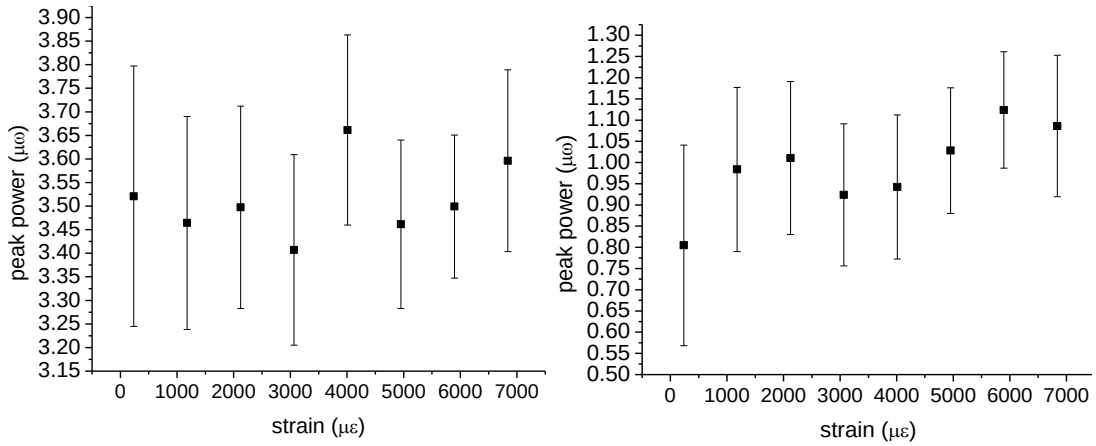

(c) (d)

Fig 4. 3. (a), (b), (c), (d) are the peak power changes from peak 1 to peak 4 in the strain experiment.

We used a linear fit for the four peaks. For peak 3 and peak 4 the standard errors are comparable or even larger to the slope of the linear fit. This means that they are no longer linearly related anymore and remains almost unchanged. It should be noted that the peak power will vary with the pulse and laser powers, pulse width, fiber length and attenuation. So the peak power may not be stable. And this has caused some deviation between the experimental results and the theoretically expected linear relations.

Since SMF is a weakly guiding acoustic fiber, (except for the transverse-type modes) there also exists another set of modes which are leaky such that their propagation constant is complex. These modes are mostly longitudinal and denoted as L_{nm} [76]. It is reported that in G_eO_2-doped-core single-mode fiber the longitudinal L_{0m} mode mainly interact with the HE_{11} optical mode [77]. Most of the displacement field of the acoustic leaky mode L_{01} is confined in the core and hence this acoustic mode scatters the optical LP_{01} mode effectively. The rest of the peaks come from the scattering from higher order acoustic leaky-core modes. Since the overlap integral between the displacement field of

the first order acoustic mode and the light intensity is largest, the first order has the highest power [11]. Subsequently the L_{01} acoustic mode will interact most efficiently with HE_{11}.

As a result of the refractive index profile difference of LEAF and SMF-28e (step-index profile), only the first acoustic mode has the highest overlap with the optical mode [1] in SMF-28e. Higher order acoustic modes have much smaller Brillouin gain, as a larger value of the acousto-optic effective area means a smaller overlap between the acoustic mode and the optical mode [10]. Hence, only one Brillouin peak is observed. For LEAF (the second fiber in [1]), the overlapping area of the first three acoustic modes are comparable with the optical effective area and they have more contribution to the Brillouin gain spectrum. High order modes are associated with waveguide properties, and they have different strain dependence. From the calculated values of the acousto-optic effective area in [1] for LEAF fiber, higher order modes have much larger acousto-optic effective areas than the first acoustic mode. So the Brillouin gain coefficients of higher order modes are much smaller.

For the 1GHz detector used, it has a noise equivalent power value of 20pw/ $(Hz)^{0.5}$. So the minimum optical power required to obtain a unity SNR is about 0.63 μw. For peak 3 and peak 4 the measured power are in 3 and 1μw ranges. Since we get the power after an electrical amplifier, the actual power should be lower than these values. As these values are so low compared with 0.63μw, it is hard to observe the linear relations for peak 3 and peak 4.

It has been reported that there is no influence on the Brillouin linewidth when the

fiber is subjected to strain [75]. However, this is not the case in LEAF fiber. Fig 4.4. shows the change of line-width under different strain.

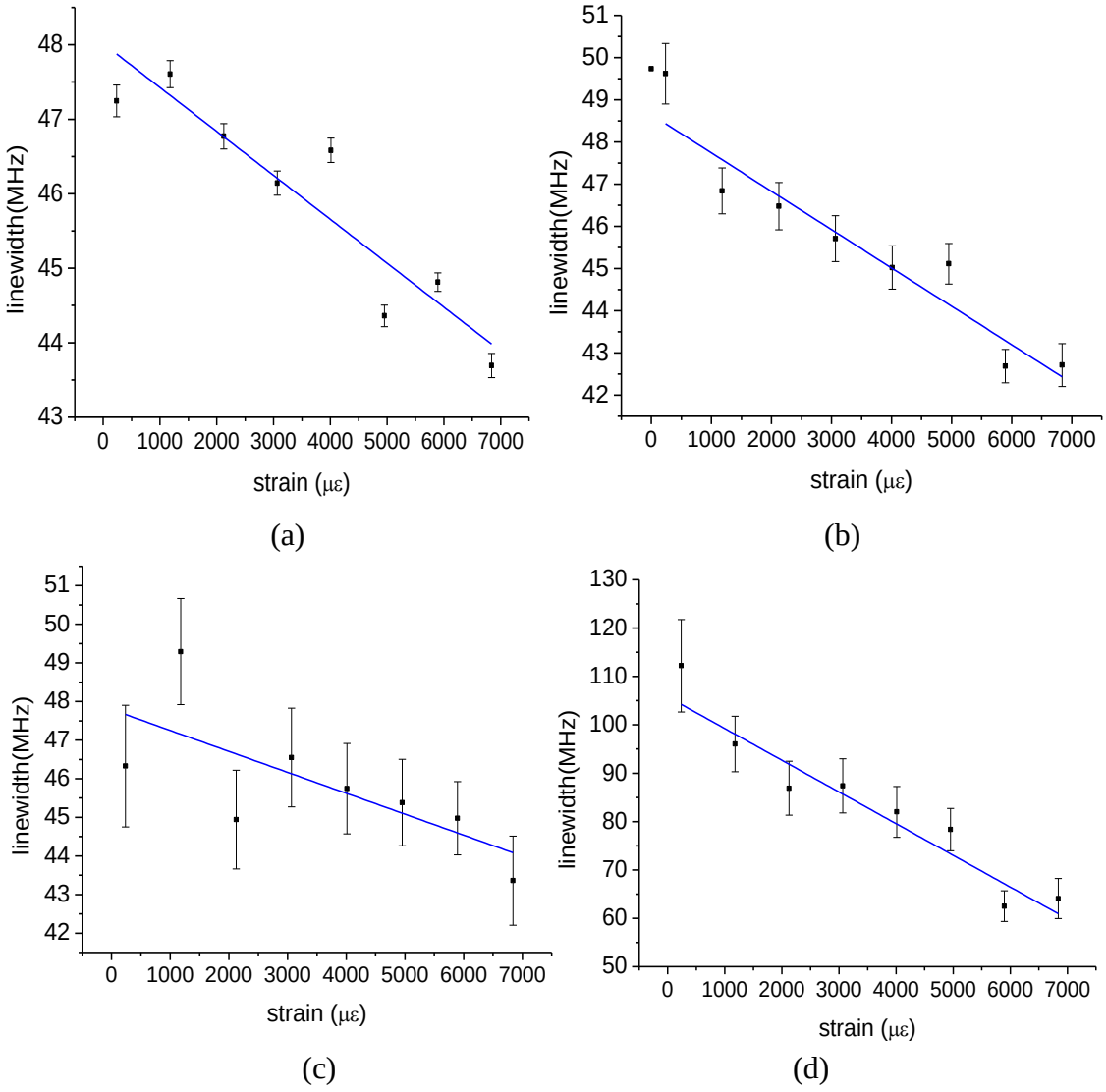

Fig 4. 4. (a), (b), (c), (d) are the linewidth changes from peak 1 to peak 4 in the strain experiment.

It is reported that for SMF-28 when the pulse power is 30mW and pulse widths are of 100 and 200 ns, there was a very slight decrease in the linewidth as the strain increased [72]. However, the variation in the linewidth over a 4000με range was less than 0.05MHZ. This made the linewidth change undetectable for a system of 30dB SNR. Hence, in the

experiment the linewidth change could not be observed for SMF-28.

If we consider the acoustic wave guide in LEAF fiber, the conventional effective area A_{eff} should be changed to A_m^{ao} which is the acousto-optic area associated with the m^{th} acoustic mode [10]. Since g_{B0} and the acousto-optic area changes with increasing strain, a nearly linear dependence on strain is found for each of the four acoustic modes. As the waveguide contribution in LEAF fiber is bigger than that in SMF, the linewidth variation with strain is much easier to observe.

4.3.3 Temperature Experiment

When the temperature increases, the volume of fiber will increase. This induces the reduction in the density of fiber.

Besides, the refractive index of silica is linearly dependent on the temperature of the fiber [78] [79]. The acoustic velocity's dependence on temperature can also be solved using the V_B and refractive index's dependence on temperature [72].

Due to these parameters' dependence on temperature, the expression of Brillouin loss peak power can be extended in terms of temperature. It was mentioned that the temperature dependent terms can be approximated to be quadratic with respect to temperature [72].

In the small range of temperatures from 20 to 70 ^{o}C, a linear approximation of the temperature dependent terms are expected. So for the Brillouin peak power, the linear relationship with temperature is also predicted in this range of temperature. It is also

shown that the Brillouin peak power is increasing with increasing temperature both theoretically and experimentally for SMF-28 [72].

In the temperature experiment, it is clearly seen that the peak power dependence on temperature is not linear after 70° C and a polynomial fit was used as shown in Fig 4.5. The tendency of peak power change is almost the same as in SMF. Since we used the 350 MHz AC detector, the noise equivalent power value is 7.4pw/(Hz)$^{0.5}$. So the minimum optical power required to obtain a unity SNR is about 0.138 μw. The electrical amplifier was not used this time. Therefore, the last two peaks have much smaller SNR than the first two peaks, and this produced some error in their power measurement. Only the first two peaks have the most observable quadratic relation on temperature.

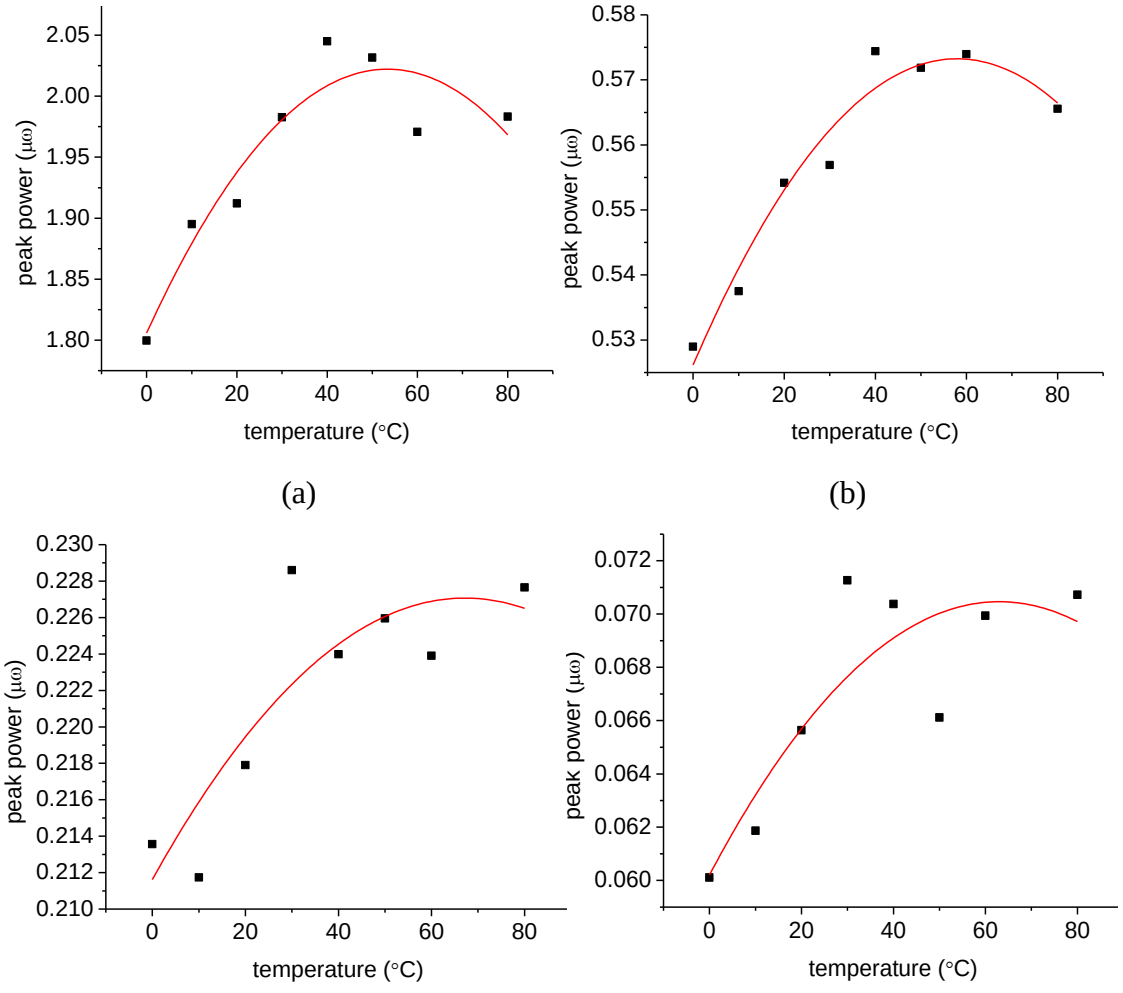

(c) (d)

Fig 4. 5. (a), (b), (c), (d) are the peak power changes from peak 1 to peak 4 in the temperature experiment.

Fig 4.6. illustrates the linewidth's temperature dependence. The linewidth's decrease is attributed to the sound wave absorption peak at low temperatures [75]. For pure silica this absorption peak occurs at around 100K. In our experiment the temperature changes from 0 ℃ to 80 ℃ which is just in the tail of the absorption spectrum. Thus, the linewidth narrowing for the first three peaks was observed. While for the last peak, since the interaction between L_{04} acoustic mode and HE_{11} optical mode is very weak, the sound wave absorption has little effect on the linewidth change of the fourth peak. In SMF-28, the linewidth is also decreasing with increasing temperature [75]. This is because SMF-28 and LEAF are both single mode fiber made of silica and the linewidth narrowing with temperature is characteristic of silica.

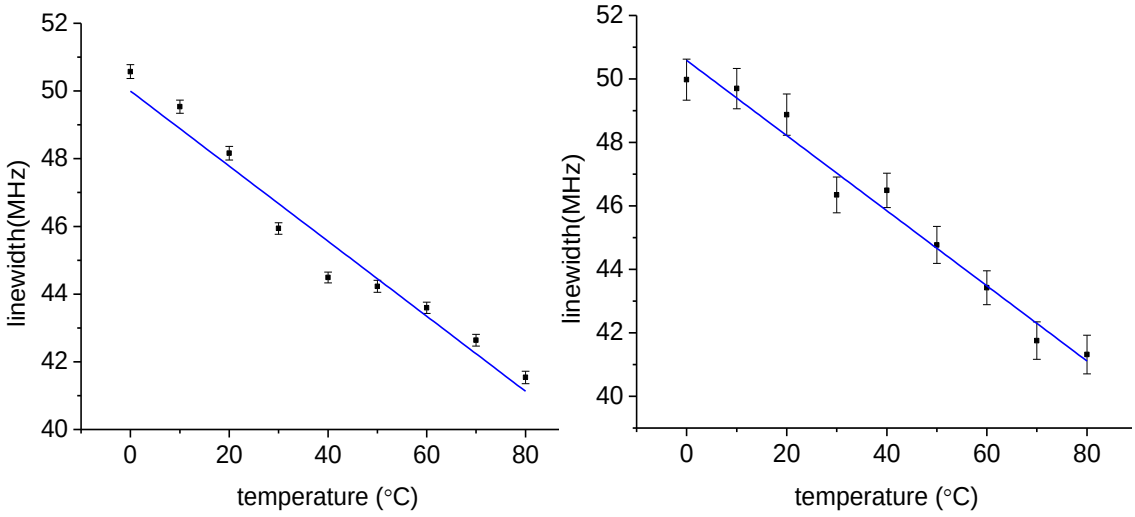

(a) (b)

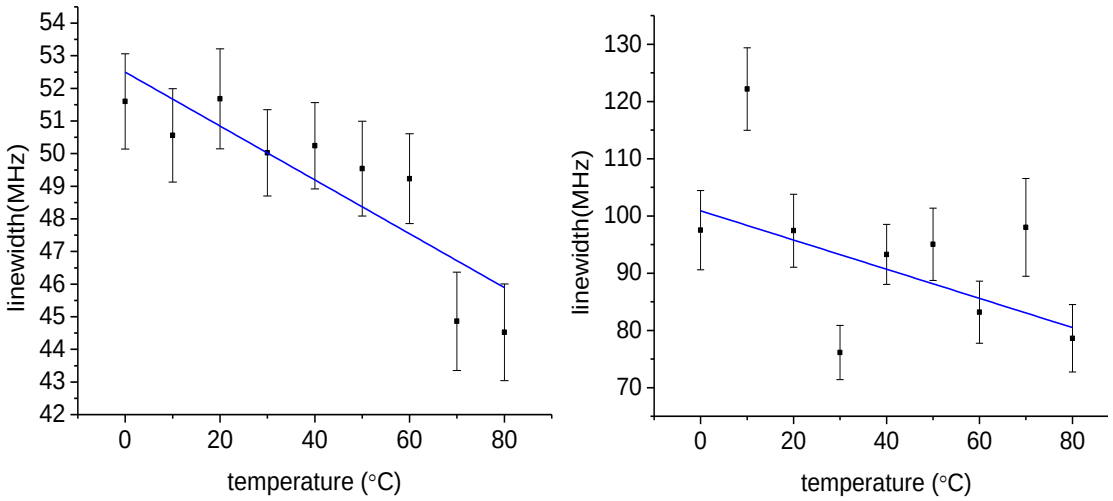

(c) (d)

Fig 4. 6. (a), (b), (c), (d) are the linewidth changes from peak 1 to peak 4 in the temperature experiment.

Fig 4.7. shows the central frequency change when strain and temperature change. The change of the coefficient under temperature is bigger than under strain, and the first two peak's central frequency strain dependence is almost the same.

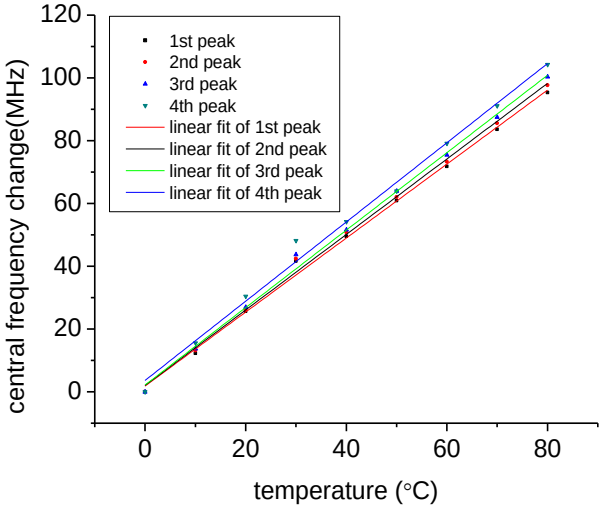

(a)

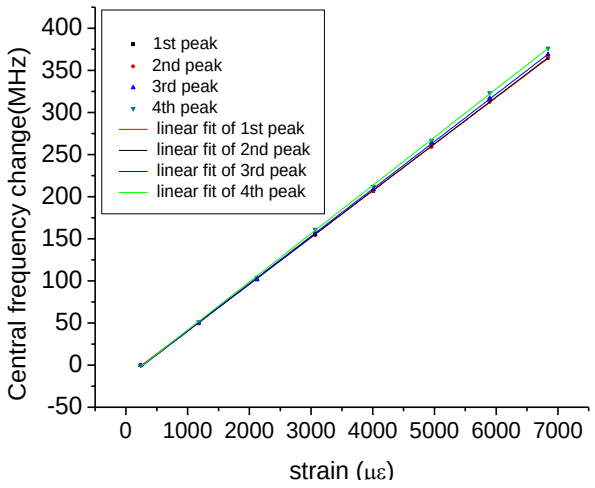

(b)

Fig 4. 7. (a) and (b) are the central frequency change for temperature and strain

When the strain is 3066με, the frequency shift of the first 45m is shown in fig 4.8.(a). The frequency shift of loose SMF28e is about 12.8GHz while this value is about 12.7GHz for the first peak of strained LEAF fiber, so we see the first sharp drop at location of 4m. The red line represents for the transition stage between different fibers (LEAF and SMF28e). This section cannot be fitted using Lorentz curve fitting. The spatial resolution is determined by 4m of the stressed LEAF fiber section which is showed in blue line, and then it is followed by another transition region. Both of transition regions have 4m length which is consistent with 40ns pulse length. The third blue line represents the V_B of the first peak of loose LEAF. Fig 4.8.(b) shows the first 300m of the sensing fiber when the oven's temperature is 60°C. Here the red line also represents for the spatial resolution which is also 4m.

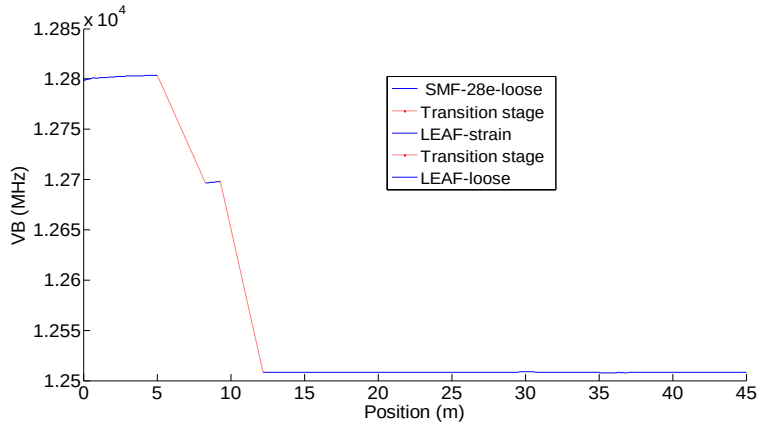

(a)

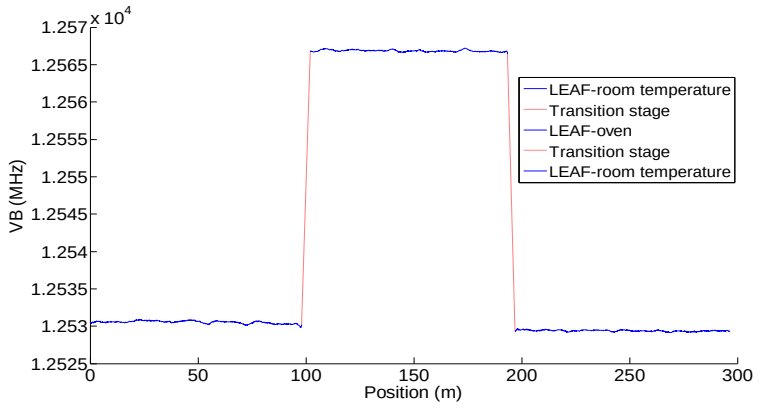

(b)

Fig 4. 8. (a) and (b) are the Brillouin frequency shift of strain and temperature in different fiber positions

4.3.4 Calculation Results

Since the linewidth has an approximately linear relationship in both strain and temperature situations, we calculated the temperature and strain errors using every peak's Brillouin frequency shift V_B and linewidth which are shown in table 4.1.

Table 4. 1. Strain and temperature error calculations using v_B and Δv_B

Peak 1					
$C\varepsilon(V_B)$ (MHz/με)	$C_T(V_B)$ (MHz/ ℃)	$C\varepsilon(W)$ (MHz/με)	$C_T(W)$ (MHz/ ℃)	S-error (με)	T-error (℃)
0.055	1.18	-0.00059	-0.111	37	1.8
Peak 2					
$C\varepsilon(V_B)$ (MHz/με)	$C_T(V_B)$ (MHz/ ℃)	$C\varepsilon(W)$ (MHz/με)	$C_T(W)$ (MHz/ ℃)	S-error (με)	T-error (℃)
0.055	1.20	-0.00091	-0.118	120	6.1

Following the error analysis reported by Jones [80] we have

$$\delta T = \frac{\left|C_\varepsilon^w\right|\delta\nu_B + \left|C_\varepsilon^{\nu_B}\right|\delta w}{\left|C_T^w C_\varepsilon^{\nu_B} - C_\varepsilon^w C_T^{\nu_B}\right|} \tag{4.9}$$

$$\delta\varepsilon = \frac{\left|C_T^w\right|\delta\nu_B + \left|C_T^{\nu_B}\right|\delta w}{\left|C_T^w C_\varepsilon^{\nu_B} - C_\varepsilon^w C_T^{\nu_B}\right|} \tag{4.10}$$

The smallest S-error and T-error are 37 με and 1.8°C , which means a more accurate measurement than 570 με and 27°C (the spatial resolution is not mentioned) in [61], 83 με and 3.9°C with spatial resolution of 15cm in [62] and 82 με and 4°C for F-B type PANDA in [63]. Furthermore, it is comparable with 44 με and 1.8°C with fiber length of 4.74m in [64]. Our spatial resolution is 4m with standard communication fiber.

The first peak's linewidth and Brillouin frequency is used for the simultaneous temperature and strain measurement. The Brillouin frequency accuracy for both temperature and strain measurement is 0.05 MHz corresponding to 1με accuracy for strain measurement, and it corresponds to a 0.04 ℃ temperature resolution. The linewidth accuracy in the strain experiment is 0.16 MHz while the linewidth accuracy in the temperature experiment is 0.18MHz. In (4.9) and (4.10), the important parameters are the changing slope, which gives the accuracy of the Brillouin frequency and linewidth.

Because of small differences for coefficients in the matrix, the recovered temperature and strain resolutions are much larger than the single parameter (temperature or strain), measurement. Hence a large pulse width (40ns) has been used.

Using a shorter pulse width or a shorter stress section (less than spatial resolution) would lead to a lower measurement accuracy on the Brillouin peak frequency and linewidth due to lower SNR, and hence a lower accuracy in temperature and strain is expected.

4.4 Conclusion

For LEAF fiber, we found that when the strain increases the first two peaks' peak power will decrease while the third and fourth peaks' peak power do not change, and the four peaks' linewidth will all decrease which is different to SMF-28. When temperature increases the four peaks' peak power will have a quadratic dependence on temperature, and their linewidth decreases with increasing temperature which is similar to SMF. The central frequency shift and linewidth of each peak were used to calculate the temperature and strain errors for simultaneous detection. The performance of a strain error of 37με and temperature error of 1.8℃ with a spatial resolution of 4m has been achieved. In practice with the measured Brillouin peak and linewidth coefficients for temperature and strain in Table 4.1 and equation（4.9）and（4.10）, simultaneous temperature and strain can be realized with LEAF fiber.

Chapter 5

Polarization Dependence of the Brillouin frequency shift of LEAF fiber

The polarization effect in optical fiber has been studied extensively. Due to the existence of fiber birefringence, a lot of applications in fiber sensors were explored. The study of the polarization in the process of SBS was mainly focused on its effect on Brillouin gain. In fact, it also changes the Brillouin frequency shift even if there are no temperature or strain variations due to the fiber non-uniformity. Although the changes are not so large quantitatively, it limits the frequency resolution in the temperature and strain sensor applications. In this chapter, we verified the input SOP's (State of Polarization) effect on the Brillouin frequency shift and also the Brillouin linewidth of LEAF fiber in the spontaneous regime. Moreover, we also compared the effects on both the Stokes and anti-Stokes cases.

5.1 Polarization Mode Dispersion (PMD)

There are two degenerate modes that are polarized in two orthogonal directions in a single mode fiber. When the fiber is perfectly cylindrically symmetric and stress-free, the mode excited in these two directions will not couple with each other. However, due to the

noncircular fiber core and nonsymmetrical stress owing to the material in the fiber preform, the mode degeneracy is broken [9]. As a result, the two orthogonal propagation modes HE_{11}^{x} and HE_{11}^{y} in a single mode fiber may travel in different group velocities due to the birefringence in the fiber [47]. The time delay between these two orthogonally polarized modes is [47]

$$\Delta\tau = \frac{(n_{//} - n_{\perp})}{c} L = \frac{L\Delta n_{eff}}{c} \tag{5.1}$$

Here $n_{\perp}$ and $n_{//}$ are the effective refractive indices of the two polarization modes. L is the fiber length. This time delay is the differential group delay (DGD) of the fiber. Since DGD is a random process, it has a probability density distribution which is the so called probability density function (PDF). A Maxwellian distribution can be used to describe the PDF [81]. The mean DGD over a unit length of fiber is defined as the PMD parameter [47]. PMD and DGD are studied [82] and measured experimentally [83].

The physical parameters: ultrasonic fields, pressure wave, temperature, strain, etc. cause the variation of fiber birefringence [84]. As a result, the output light intensity will change with time and position following the disturbance. Therefore, the fast changes in aerial [85] and submarine fibers [86] due to the wind, sun radiation and wave changes can be detected. Furthermore, in order to compensate the polarization mode dispersion in the transmission direction, the electrical current changes in optical ground wires(OPGW) can also be measured using this method [87].

5.2 Polarization Effect on SBS

So far, the research of polarization effect on SBS has been concentrated on the Brillouin gain [88] [89]. A polarization averaging technique was introduced to remove the contrast fluctuations caused by the polarization change [90]. Applying two successive measurements of the Brillouin gain with two different particular states of polarization, the actual Brillouin gain coefficient of a piece of fiber can be measured when the polarization is neither preserved nor completely scrambled [75]. Recently, a polarization pulling effect is demonstrated experimentally [91]. It was mentioned that both the fiber birefringence and local SBS interaction controlled the evolution of the signal SOP. Due to the SBS interaction, the amplified Stokes wave's SOP will converge to the state of the maximum amplification.

As a matter of fact, the peak Brillouin frequency is also affected by the PMD effect. A sensor's accuracy of temperature or strain measurement is mainly determined by the Brillouin frequency resolution. The Brillouin scattered light has a frequency shift as follows [21]

$$\upsilon_B(z) = \frac{2n_{eff}(z)v_a}{\lambda} \tag{5.2}$$

where n_{eff} is the effective mode refractive index of the fiber as a function of distance z. The velocity of sound in glass is v_a and λ is the free-space wavelength. The change of temperature and strain will mainly induce the change of acoustic velocity instead of the refractive index of fibers. So when the effective refractive index varies, even if the temperature and strain is constant, the Brillouin peak frequency will change across

different fiber sections. Obviously, the Stokes and anti-Stokes frequencies changes will be different because n_{eff} is different in these two cases as the effective mode refractive index depends on the frequency.

In sum, the temperature and strain resolution should be the combination of the following two contributions [21]

$$\delta\nu_B(z) = \delta\nu_{B,SOP}(z) + \delta\nu_{B,SNR}(z) \tag{5.3}$$

In this chapter, we measured the peak Brillouin frequency change and the Brillouin linewidth change of LEAF fiber in both the Stokes and anti-Stokes regimes when we adjust the SOP of the input light. The results showed that the Brillouin peak frequency and Brillouin linewidth would change when the SOP changes. And we also got the range of these variations.

5.3 Experimental Setup

The experimental setup is shown in figure 5.1. The optical power of the laser source (with angular frequency of $\omega_\circ$) is separated into two parts. 95% of the power is attenuated by an attenuator at first and then passes through the isolator and the polarization controller. The circulator is used to direct the light into the fiber under test. The reflected light with both Stokes and anti-Stokes shifts are selected by FBG1. This filter can be tuned to allow only Stokes or anti-Stokes waves to pass at one time. FBG2 is used to remove the amplified spontaneous emission (ASE) noise produced by EDFA1. On the other hand, 5% of the laser power is incident into EOM which is modulated by a

tunable RF source to produce two sidebands with angular frequency of ω_0-Ω_{RF} and ω_0+Ω_{RF} respectively. The DC bias voltage of the modulator bias controller can be set to eliminate the part with frequency of ω_0. The EDFA2 is used to amplify the signal while FBG3 eliminates the amplified ASE noise. Using the heterodyne coherent detection, the two parts of the optical power are combined at the 50:50 coupler and then detected by a 1GHz AC detector. Then the spectrum is displayed in the electrical spectrum analyzer (ESA). The length of LEAF fiber is 6.3km. The pump power at circulator's port 1 is 5 mW.

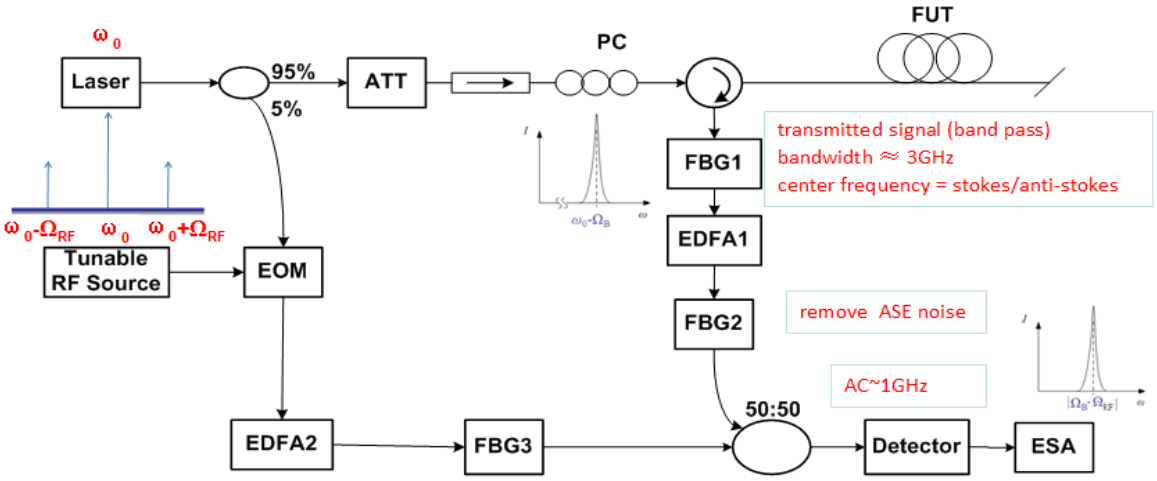

Fig 5. 1. Experimental setup (FUT: 6.3km LEAF fiber)

5.4 Experimental Result-Stokes

Since the RF source frequency is set to be Ω_{RF} =10400MHz, the frequency shown on the ESA is actually Ω_B - Ω_{RF}. When we are performing the data processing, Ω_{RF} is added to get the real spectrum. Then for each peak of the Stokes spectrum, we measured the Ω_B change range by rotating the three paddles of the polarization controller 97 times.

We got the value of Ω_B by doing the Lorentz curve fitting for each of the four peaks respectively and they are shown in fig 5.2. The amplified spectrums are also shown from peak 2 to peak 4.

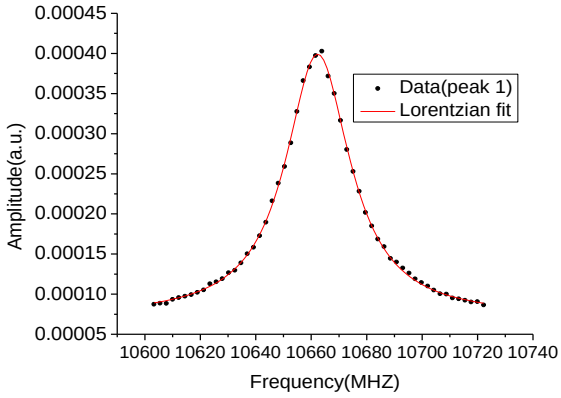

(a)

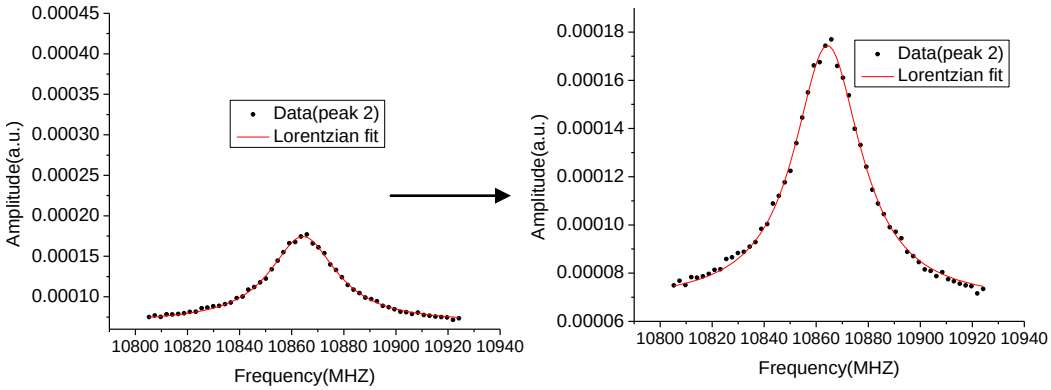

(b)

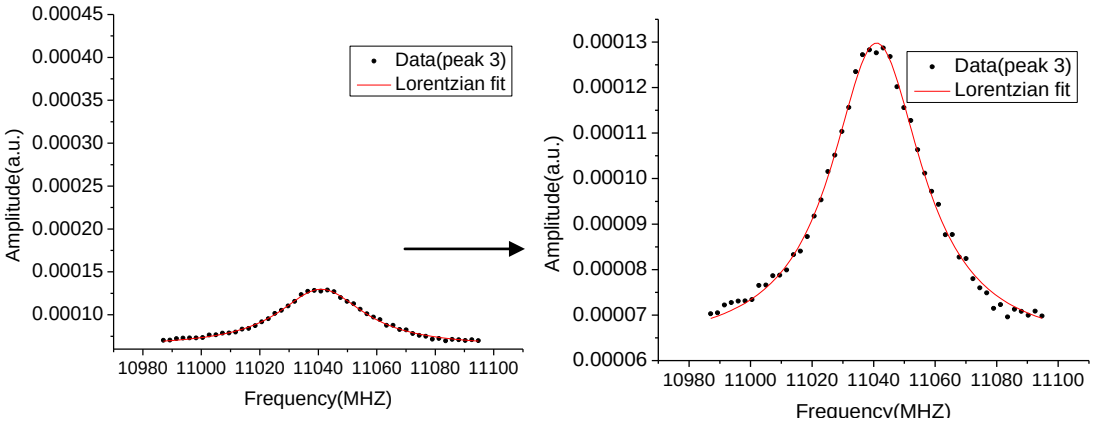

(c)

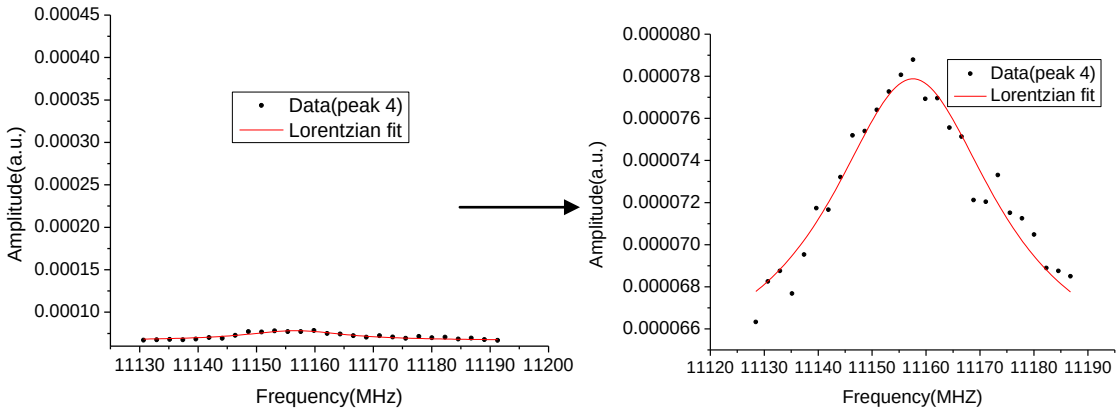

(d)

Fig 5. 2. Lorentz curve fit of the Stokes spectrum: (a), (b), (c), (d) are for peaks 1 to 4.

Table 5.1 shows the four peaks' Stokes Brillouin frequency and linewidth change. We found that the linewidth was also altered by the input light's SOP. Since the fitting uncertainty for the 97 times are different but close to each other, we take the average uncertainty. If we only look at the V_B change range, peak 1 has the smallest value while peak 4 has the largest value. However, this value cannot be taken as a criterion for the sensitivity of each peak's V_B on the input SOP because the V_B change largely depends on the constant value of the velocity of sound. Therefore, we used the probability density spectrum to find the sensitivity dependence for all the peaks.

Table 5. 1: the four peaks' Stokes Brillouin frequency and linewidth change

Peaks	Mean V_B (MHz)	V_B Change Range (MHz)	V_B Average Uncertainty (MHz)	Mean Linewidth (MHz)	Linewidth Change Range (MHz)	Linewidth Average Uncertainty(MHz)
Peak 1	10662.4	0.4	0.05	28.08	3.60	0.25
Peak 2	10864.2	0.5	0.10	31.77	3.32	0.50
Peak 3	11040.9	0.7	0.16	35.16	3.59	0.85
Peak 4	11156.7	4.3	0.72	25.63	21.09	4.98

For the first peak, since (V_B change)/ (average uncertainty) =6.7, we divided the change range into six equal sections. For the second peak, as (V_B change)/ (average

uncertainty) =5.0, five equal sections were divided. For the third peak, the value of (V_B change)/ (average uncertainty) =4.5, the divided sections were four. As for the fourth peak, (V_B change)/ (average uncertainty) =5.9, we divided the change range into six equal sections. We then counted the frequency's appearance times for each of the sections. To get the probability for these sections we divided each of them by 97. The probability spectrums are shown in figure 5.3. In the x axis, zero represents for the minimum V_B. We tried to fit the probability density spectrum using the Maxwellian distribution which is valid for DGD. However, it cannot be fitted. It may be caused by the insufficient data since we only tuned the SOP for 97 times which are far less to cover the entire Poincare sphere. The other reason is that the distributions of Δn_{eff} and n_{eff} may be totally different.

We can see that the most probable change of V_B from the minimum V_B is around 0.2~0.25MHz which corresponds to 10662.4~10662.4 MHz for the first peak. For peak 2, the most probable change of V_B from the minimum V_B is around 0.2~0.3MHz which lies in the range of 10864.1~10864.2 MHz. For peak 3, the most probable change of V_B from the minimum V_B is around 0.2~0.35MHz which means 11040.8~11040.99 MHz. For peak 4, the most probable change of V_B from the minimum V_B is around 1.5~2MHz which corresponds to 11156.5~11157.01MHz.

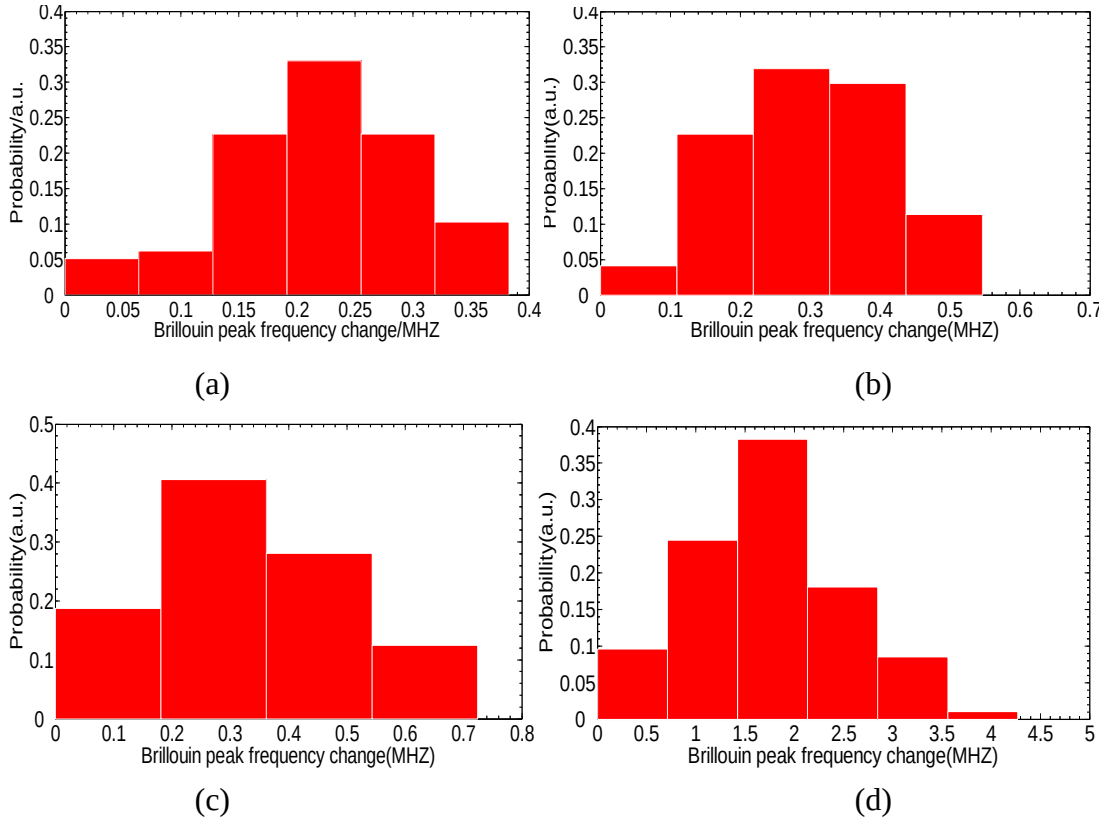

Fig 5. 3. (a), (b), (c) and (d) show the Stokes V_B change probability histograms from peak 1 to 4.

Since the (linewidth change range)/(linewidth uncertainty) is 14.60, 6.59, 4.20 and 4.23 for peak 1 to peak 4 respectively, following the same process in the Brillouin peak frequency we also divided the Brillouin linewidth change range into 14, 6, 4 and 4 sections for the four peaks. The result is shown in fig 5.4.

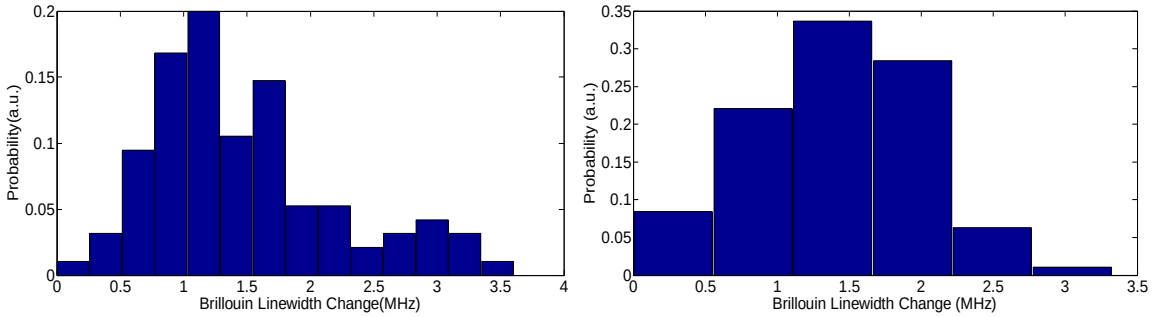

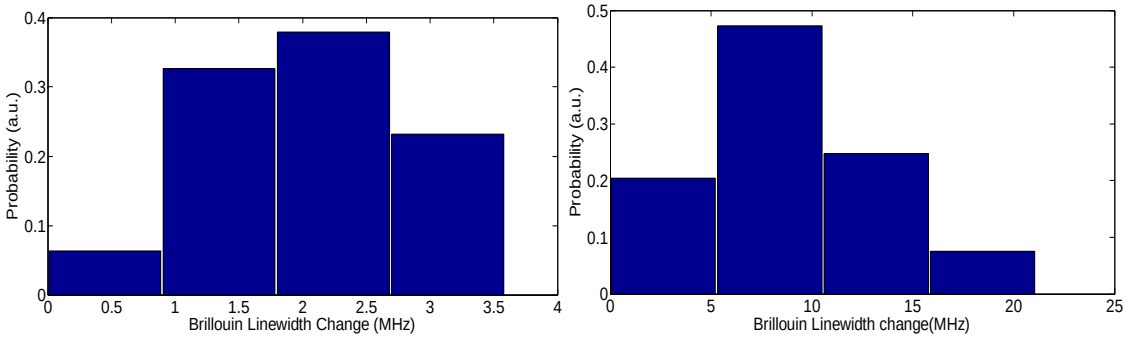

(c) (d)

Fig 5. 4. (a), (b), (c) and (d) are the probability density spectrum of Brillouin linewidth from peak 1 to peak 4 for Stokes scattering

These figures demonstrated that the Brillouin linewidth has a very different behaviour from the Brillouin peak frequency especially for the first peak. In figure 5.3 (a), the Brillouin peak frequency is first increased to the peak value and then gradually decreased which is very uniform. In figure 5.4 (a), at first the linewidth is indeed increased to the largest value. However, the Brillouin linewidth is decreasing non-uniformly. It can be seen that the first peak's Brillouin linewidth also has the largest dependence on the input SOP which is in common with the trend of Brillouin peak frequency. When the light is launched in the principle state of polarization (PSP), it is much easier to build Brillouin amplification. In this case, the linewidth should be narrower. When the SOP is far from PSP, the linewidth should be maximum. This explains why the linewidth also has a dependence on the input light's SOP.

In conclusion, the most probable change of V_B from the minimum V_B are around 0.2MHz for the first three peaks. The first peak has the greatest dependence on the polarization state of the input light because of the largest ratio of (V_B change)/ (average

uncertainty). As we have demonstrated in chapter 3, the first peak has the smallest acousto-optic effective area [1] which means a larger overlap between the acoustic mode and optical mode. Therefore, the first peak's V_B varies most sensitively with the input light's SOP. Although the fourth peak's ratio of (V_B change)/ (average uncertainty) is bigger than the second and third peaks, it is just because the fourth peak's sound velocity is much larger than the other three peaks and a very slight change of the n_{eff} will induce a much larger variation of V_B.

5.5 Experimental Result-anti-Stokes

For the anti-Stokes case, we also used the Lorentz curve fit to fit the four peaks. The spectrums of the four peaks are demonstrated in fig 5.5. It can be seen that the first three peaks can be well fitted with the Lorentz curve as almost all the data points are on the fitted curve. For the fourth peak, the data points are much more distracted. However, it can also be fitted using the Lorentz curve fit with a larger fitting error. In the anti-Stokes case, the peaks' power seem to be larger than in the Stokes case which is contrary to the experimental result in [49]. This is because we used the coherent detection with a higher power for the local oscillator while they applied the direct detection with an optical high-resolution spectrometer.

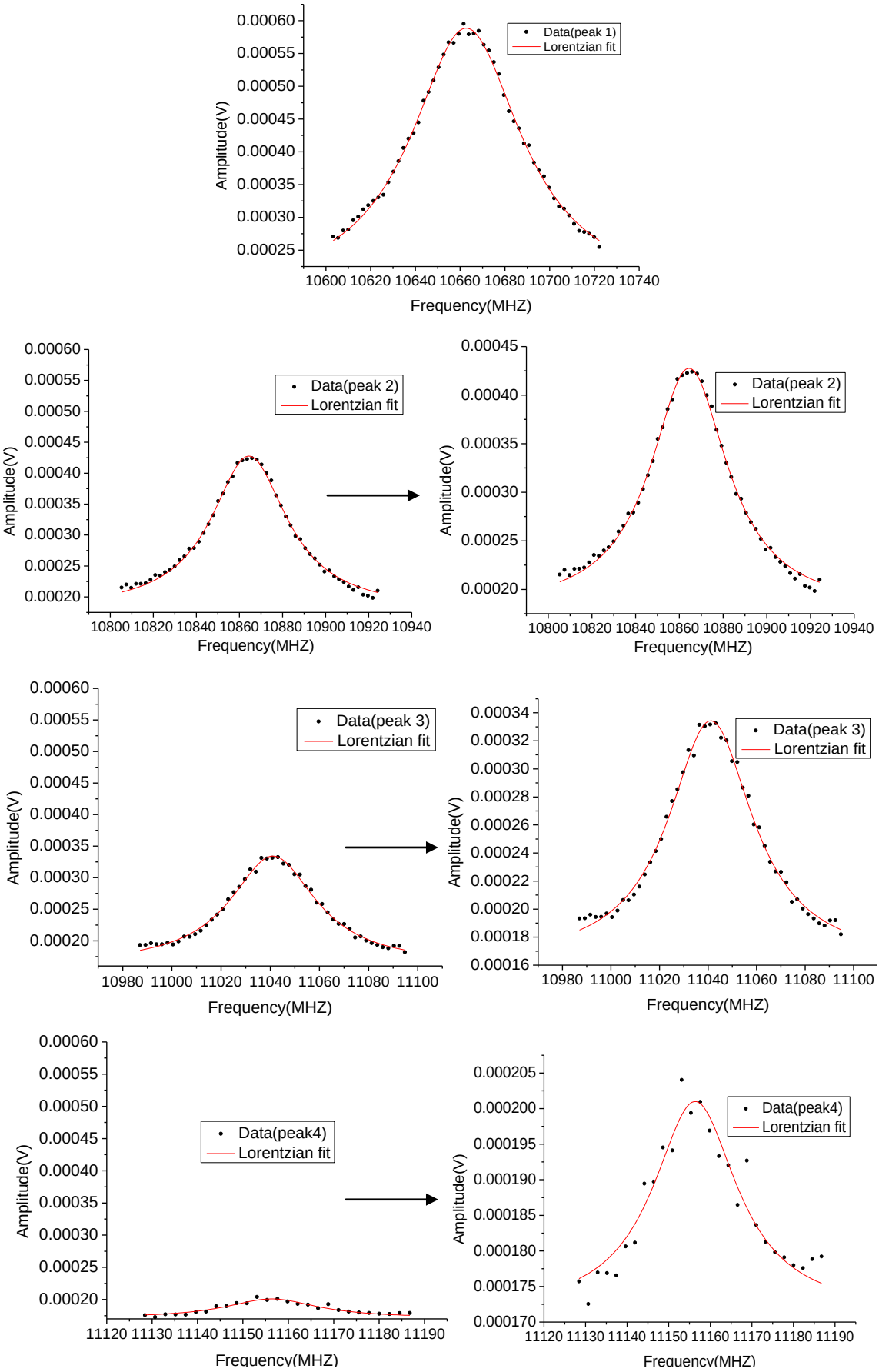

Fig 5. 5. Lorentz curve fit for the four peaks of the anti-Stokes spectrum.

Table 5.2 shows the anti-Stokes Brillouin frequency and linewidth change of the four peaks. Although the V_B change ranges for the first three peaks appear to be larger in the anti-Stokes case than in the Stokes case, the average uncertainty is also larger. The fourth peak has almost the same average uncertainty as in the Stokes case while the V_B change range is much smaller than that for the Stokes regime. This means the fourth peak has a much smaller dependence on the input light's SOP change. We also observed that the V_B in both the Stokes and anti-Stokes cases for each of the peaks has almost the same value with the variations of less than 1MHz. The same result is also demonstrated in chapter 3 which also applied the coherent detection method. However, in the experiment of [49], there are 7MHz difference for each peaks' V_B between the Stokes and anti-Stokes cases. This distinction is caused by different detection methods. And the different values of the V_B are caused by different samples of LEAF fiber which are manufactured in different environments and at different times.

Table 5. 2: the four peak's anti-Stokes Brillouin frequency and linewidth change

Peaks	Mean V_B (MHz)	V_B Change Range (MHz)	V_B Average Uncertainty (MHz)	Mean Linewidth (MHz)	Linewidth change range (MHz)	Linewidth Average Uncertainty (MHz)
Peak 1	10662.7	0.7	0.1	56.5	15.0	1.0
Peak 2	10864.6	0.7	0.2	40.1	6.5	0.9
Peak 3	11041.4	0.8	0.2	40.4	5.6	1.2
Peak 4	11156.2	2.7	0.6	23.5	16.5	3.8

Using the same method as in the Stokes case we divided the whole V_B change range into 5, 4, 4, 4 sections for peaks 1, 2, 3, 4 respectively. We also draw the probability density spectrum for the four peaks which are shown in figure 5.6. For peak 1 the most

likely frequency change from the minimum V_B is around 0.3-0.4MHZ. And this lies in the frequency range of 10662.7-10662.8 MHz. For peak 2 the section with the biggest probability is 0.2-0.4MHZ. And this is just the range of 10864.4-10864.6 MHZ. For peak 3 the most probable section is also 0.2-0.4MHZ. This corresponds to 11041.2-11041.4MHZ. For peak 4 the section with the biggest probability is 0.7-1.4MHZ which is in the frequency range of 11155.6-11156.3MHZ. These results are different than in the Stokes case.

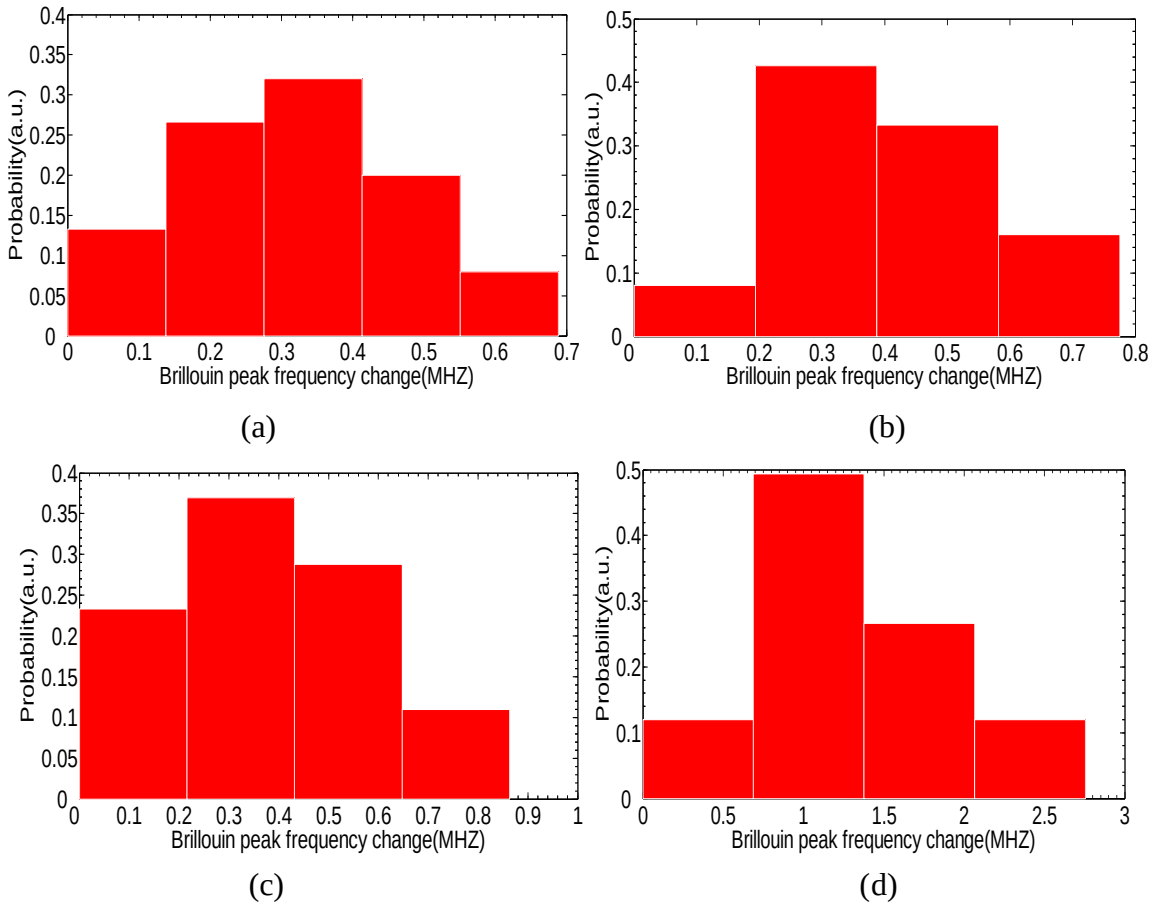

Fig 5. 6. (a), (b), (c), (d) represent for the probability histogram of peaks 1, 2, 3, 4 for Brillouin peak frequencies in the anti-Stokes case.

From the above data and figures, it can be inferred that the four peaks in the anti-Stokes case have much smaller dependence on the polarization state variation of the input light as the divided sections in the anti-Stokes case are much smaller than in the Stokes case. The most probable change of V_B from the minimum V_B are around 0.2-0.4 MHz for the first three peaks. The different behaviours between the Stokes and anti-Stokes cases are caused by the different processes they involved which were mentioned in chapter 3.

We also plotted the Brillouin linewidth's probability density spectrum in fig 5.7. The divided sections are 14, 6, 4 and 4 for the four peaks since the value of (linewidth change range) / (linewidth average uncertainty) are 14.3, 6.7, 4.4 and 4.3 respectively for peak 1 to peak 4. The number of divided sections is coincidently equal to those in the Stokes case.

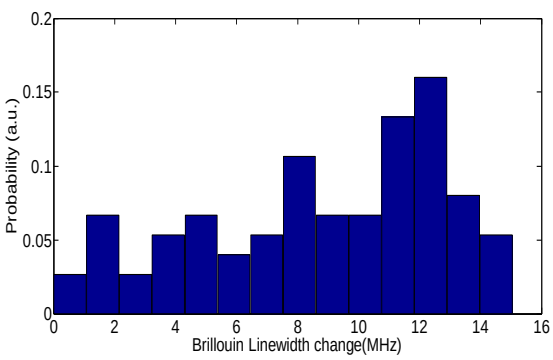

(a)

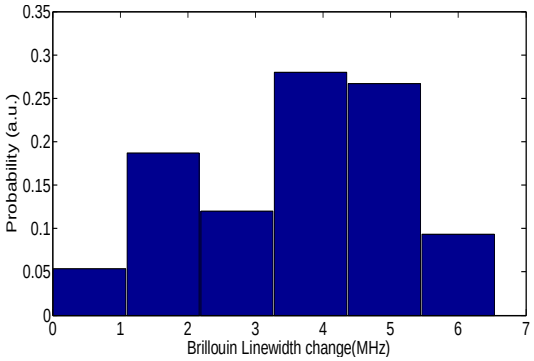

(b)

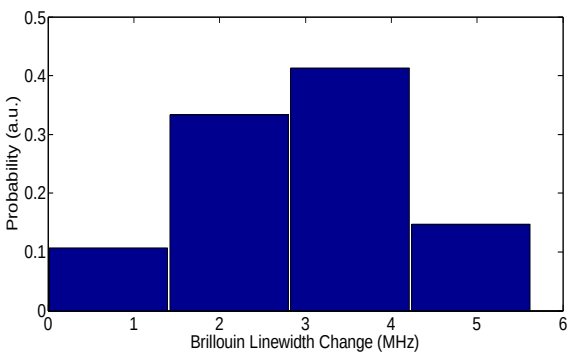

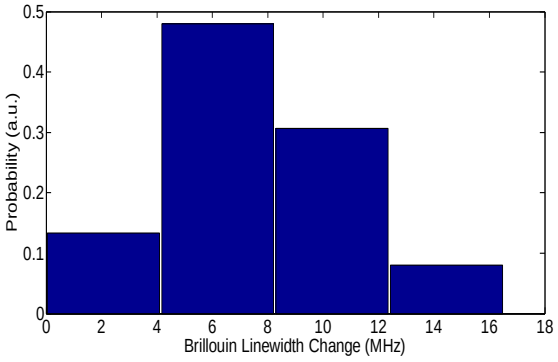

(c) (d)

Fig 5. 7. (a) (b) (c) (d) are the probability density spectrum of the Brillouin linewidth from peak 1 to peak 4 in the anti-Stokes case.

This figure indicates that peak 1 and peak 2 are non-uniform in the distribution especially for peak 1. In the anti-Stokes case, the linewidth of peak 1 also has the highest dependence on the input SOP change.

5.6 Conclusion

We demonstrated experimentally that the variation of the input SOP changes the Brillouin frequency shift and also the Brillouin linewidth of the four peaks of LEAF fiber in the spontaneous regime. In the Stokes case, the Brillouin frequency is shifted by 0.2MHz for the first three peaks. In the anti-Stokes case, the average Brillouin frequency shift is 0.2-0.4 MHz. Although this value is larger than in the Stokes cases, the fitting error is also larger. From the probability histogram of the four peaks in the Stokes and anti-Stokes cases, it is inferred that the four peaks's Brillouin frequency shift have larger dependence on the SOP change of the input light in the Stokes case. Considering the probability density spectrums of both the Brillouin peak frequency and Brillouin linewidth, the first peak has the highest dependence on the input light's SOP. After all we only tried 97 different SOPs. So the demonstrated V_B change range and the probability spectrum are just approximate. The actual range may be even larger than that in the experimental conditions.

Chapter 6

Simultaneous Temperature and Strain Measurement Using Beat Frequency of Spontaneous Brillouin Scattering in LEAF Fiber

Heterodyne coherent detection is conventionally applied to map the Brillouin spectrum in the spontaneous Brillouin scattering measurement to increase the signal to noise ratio (SNR), which complicates detection system and slows the measurement procedure. Here, we demonstrated that using direct detection of the two beat frequencies of different Brilloun peaks of LEAF fiber via spontaneous scattering one can realize the simultaneous temperature and strain measurement without mapping the Brillouin spectrum. The strain and temperature accuracies are 1) 0.4°C and 93με respectively for strain of less than 1476με, and 2) 0.3°C and 14με for strain larger than 1476 με. Here, 1476 με is a critical point and it is different for different fiber length.

6.1 Introduction

The BOTDR [92] [93] [94] is based on spontaneous Brillouin scattering and only one pump pulse is used. In BOTDR's configuration, usually the heterodyne coherent detection was applied to increase the SNR and to shift the backscattered Brillouin signal into the radio frequency range for micro-wave detection [95] [96] [97]. The coherent

detection requires swept microwave source and high frequency detection (>10 GHz) to cover the Brillouin spectrum, as well as locking of the reference and signal beam. This makes the detection system complicated and the procedure takes a longer time to gather the data. Often it only detects either temperature or strain. As the Brillouin frequency is a function of both temperature and strain, it makes simultaneous temperature and strain detection with the Brillouin peak alone difficult. To solve this problem different kinds of methods have been proposed, which have been discussed in chapter 4. However, all of those measurements require mapping of the Brillouin spectrum.

In the LEAF fiber, there are four Brillouin peaks [48], the Brillouin frequency difference between peak 1 and other peaks can be written as:

$$\Delta\Omega_{B,1-i} = \frac{2n_{eff}}{\lambda}(V_{a,1} - V_{a,i}) = \frac{2n_{eff}}{\lambda}\Delta V_a \tag{5.1}$$

Here i represents the peaks 2, 3 and 4, n_{eff} is the effective index of the LEAF fiber, λ is the wavelength of the light, and V_a is the velocity of the sound for different acoustic modes [1] . Because of the small frequency difference between the four peaks, we can take them with the same refractive index; the difference in beat frequency is mainly contributed by different sound velocities of different acoustic modes. Because of the non-uniform acoustic velocity profiles in the fiber associated with different acoustic modes, they changes at different locations due to doping concentration [98], which brings different temperature and strain dependence. Such a process is different from that of BOTDA, in which the specific frequency difference between the pump and probe wave has chosen a specific acoustic mode. In BOTDR, the pump wave at low power has excited all of the acoustic modes, and the difference between various modes and their

overlapping with the optical modes at different fiber location gives the beat frequencies which change with temperature and strain differently at different fiber location. This means we can measure the peak of the beat frequency, the height and width for their temperature and strain dependence. Using this relation one can realize simultaneous temperature and strain measurements.

In this chapter, we demonstrated that the beat frequency of the Brillouin peaks in LEAF fiber can be applied to measure temperature and strain simultaneously. Since the beat frequency is in the radio frequency range (hundreds of MHz), this lower frequency range makes it easy to get electrical amplification and low bandwidth detection. The system does not need heterodyne detection. It transforms micro-wave detection of optical and electrical signal to radio frequency detection, which significantly simplifies the detection system for making a cost effective distributed Brillouin sensor system. As the part of frequency sweeped may not be necessary and it therefore significantly saves measurement time. In our experiment, the best temperature and strain performance we can get are 0.4°C and 93με when the applied strain is less than 1475.6με while the results are 0.3°C and 14με when the strain is larger than 1475.6με. Here 1475.6 με is the critical strain that shows the different strain response between acoustic modes 1 and 2 or 3. This number is associated with non-uniform acoustic velocity profiles; hence it changes with fiber length.

6.2 LEAF Beat Spectrum

In the experiment of fig 5.1, when we tried to measure the LEAF fiber spectrum using the conventional heterodyne coherent detection method in the spontaneous regime, we found that when there was no local signal input we still observed three peaks which is apparently not the spectrum of LEAF fiber. We used the multi-peak Lorentz curve fit for the three peaks and got the peak frequencies for each of these peaks. Eventually we found that they coincidently equal to the beat frequencies between the first peak and the rest of the peaks. The frequency results are listed in table 6.1 and 6.2. We also found that these three peaks only appeared when the input power was high enough: several mW.

Table 6. 1: Brillouin frequency shift of LEAF fiber's four peaks at 1550nm

V_B (MHz) at 1550nm			
Peak 1	Peak 2	Peak 3	Peak 4
10662	10864	11041	11158

Table 6. 2: The calculated frequency differences of LEAF fiber's first peak between the other peaks and the multi-peak Lorentz curve fit results of the three peaks for LEAF beat

Beat frequencies (MHz)			
	Peak 1-2	Peak 1-3	Peak 1-4
Coherent detection	202	379	496
Direct detection	200.51	379.75	497.43

6.3 Experimental Setup

In order to use the three peaks of LEAF beat for the temperature and strain sensor, we designed the experimental setup in fig 6.1. This experiment was conducted at 1319nm wavelength. The probe laser has a maximum output power of 110mW. After passing through a section of PMF and a 99:1 coupler, the power of the laser is adjusted via the attenuator. The first 99:1 coupler is used to monitor the output power of the laser while the second one is to detect the power after the attenuator. 99% of the power from the second 99:1 coupler enters into the isolator and then into the circulator. The backscattered signal from the fiber under test (FUT) is detected by a 1GHz AC detector. When the input power into LEAF fiber is several mW, the first peak of LEAF will beat with the second peak and the third peak. Then the whole spectrum will be in the MHz range and can be easily detected by a 1GHz AC detector. The input power is 10mW which is below the SBS threshold for LEAF fiber, while the power arriving at the detector was measured at 40μW.

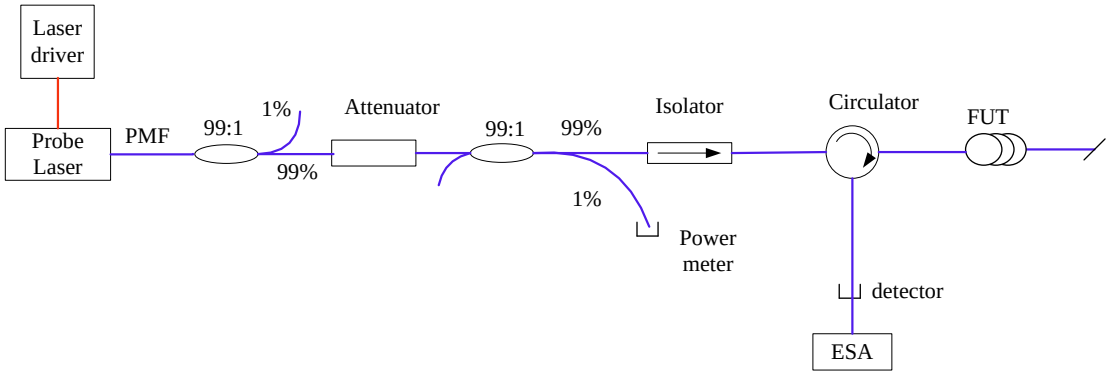

Fig 6. 1. Experimental setup of LEAF beat

The measured spectrum at room temperature is illustrated in fig 6.2.(a) while fig 6.2.(b) and fig 6.2.(c) are the Lorentz curve fit of the first and second peaks of the LEAF beat. The two peaks' spectrum can be fitted well with the Lorentz curve.

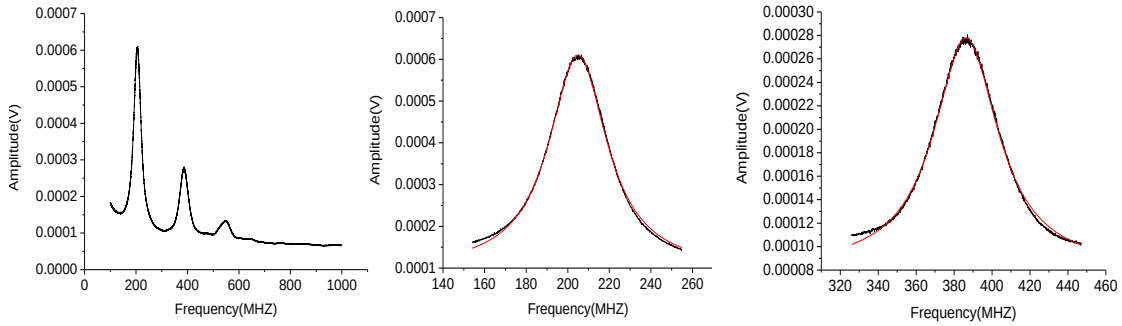

(a) (b) (c)

Fig 6. 2. (a) is the measured spectrum in ESA while (b) and (c) are the spectrum and Lorentz curve fit of the first and second peaks of LEAF beat.

6.4 Temperature Experiment

In the temperature experiment, the fiber length is 6.3km and the whole reel of fiber was put in an oven whose temperature was changed from 23.7 ℃ to 59.4 ℃. For the first and second peaks of the LEAF beat spectrum, we got their central frequencies' relationships with temperature in fig 6.3. Here we also added the error bars for each of the frequencies. We can see that the first two peaks' frequencies can be linearly fitted very well with temperature change.

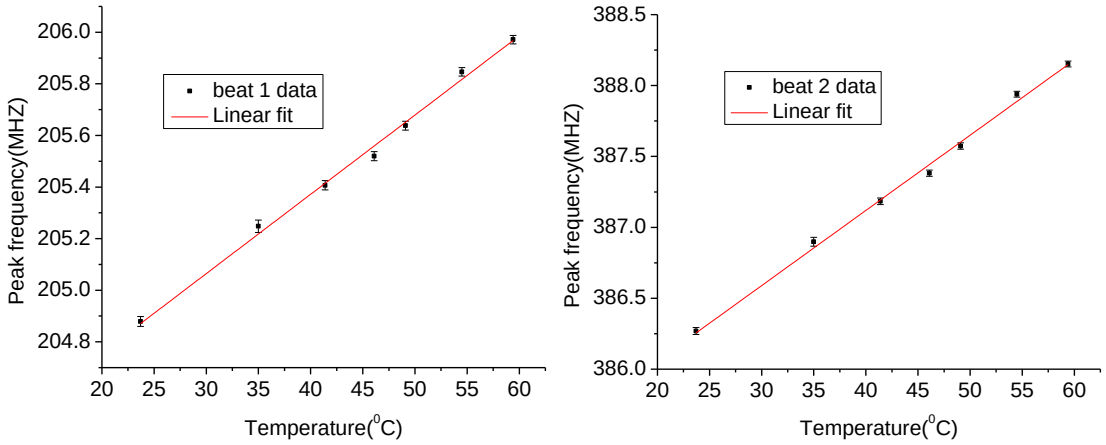

Fig 6. 3. the first two peaks' frequency relationship with temperature.

For the BOTDA system which was illustrated in chapter 4, we calculated the frequency difference between peak 1-2 and peak 1-3. Fig 6.4 shows their dependence on temperature. If the uncertainty is taken into consideration, the frequency difference changes linearly with temperature which conforms to our experimental result.

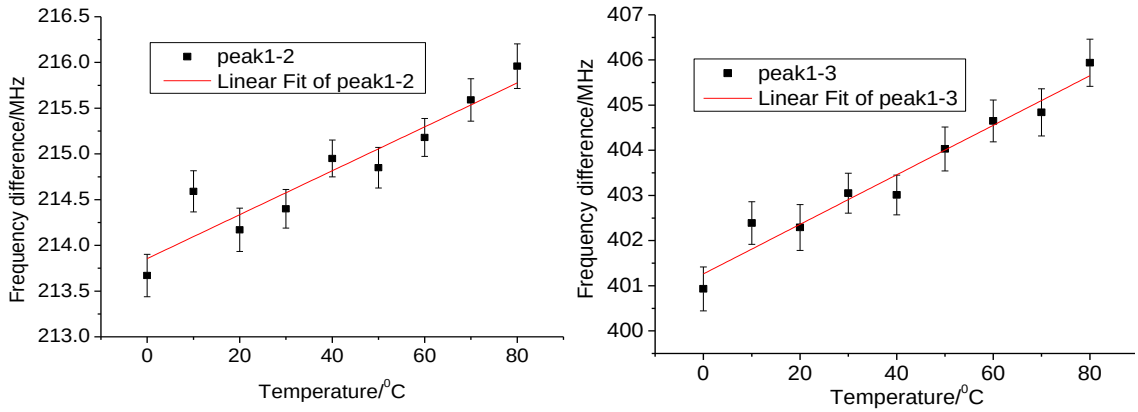

Fig 6. 4. The relationship of frequrency difference of peak 1-2 and peak 1-3 with the temperature: calculated from the results of the BOTDA system in chapter 4.

We also checked the peak power change with increasing temperature. It was found that the peak power was increasing with increasing temperature which was the same as in

chapter 4 for LEAF fiber's Brillouin peaks. The first two peaks of LEAF beat can also be linearly fit with temperature in fig 6.5.

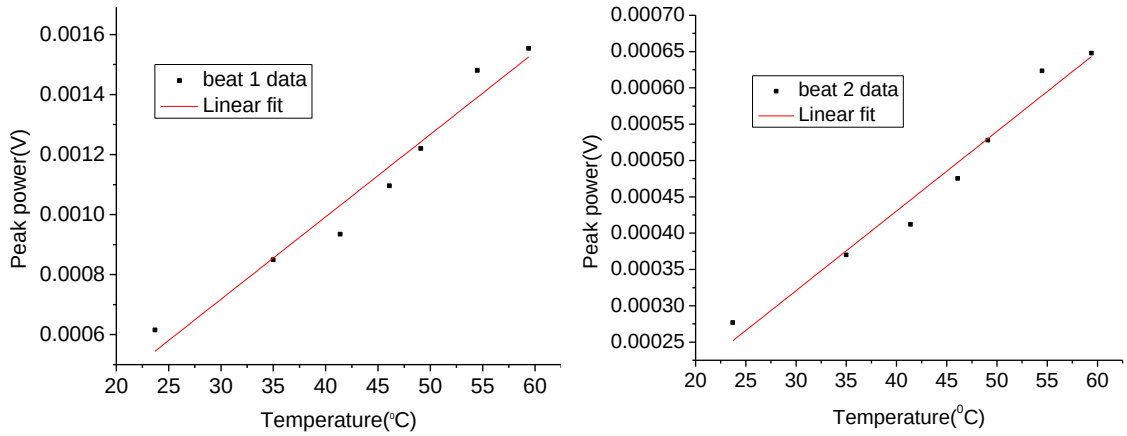

Fig 6. 5. The relationship between the first two peaks' peak power and temperature.

In fig 6.6, it can be seen that the linewidths are decreasing with increasing strain for the first two peaks. As was mentioned in [75], the temperature range in our experiment is just at the upper tail of the absorption peak for phonon absorption. Since the linewidth's decrease with increasing temperature was expected for each of the peaks of LEAF's Brillouin spectrum, the same result could be predicted for the first two peaks of LEAF beat.

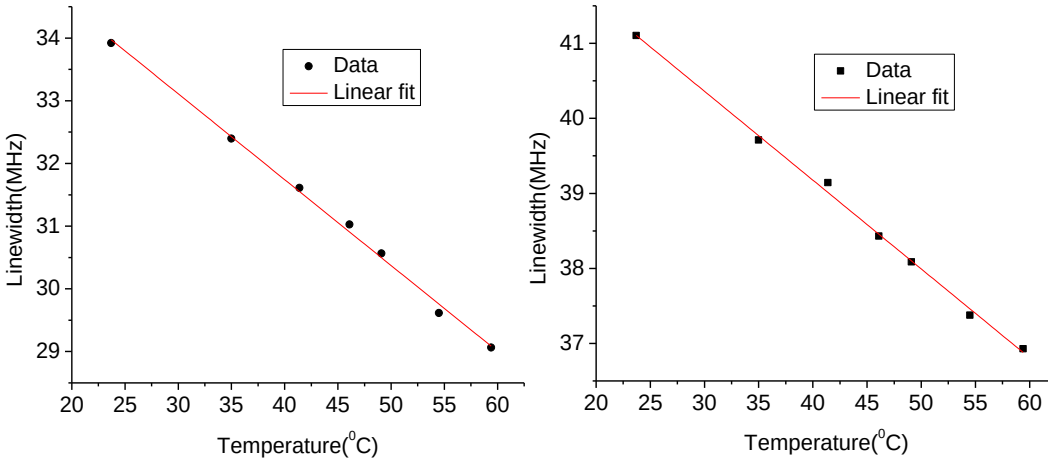

Fig 6. 6. The relationship between the first two peaks' linewidth and temperature.

Applying the linear fit to peak frequency, peak power and linewidth with temperature, we got their coefficients which were shown in table 6.3. δ_{VB}(T), δp(T) and δ_W(T) represent for the fitting error of peak frequency, peak power and linewidth.

Table 6. 3. Temperature coefficients and fitting error of peak frequency, peak power and linewidth

	$C_T(V_B)$ (MHz/ ℃)	C_T(P) (V/ ℃)	C_T(W) (MHz/ ℃)	δ_{VB}(T) (MHz)	δ_p(T) (V)	δ_W(T) (MHz)
Peak 1	0.031	2.75E-05	-0.14	0.018	7.66E-06	0.095
Peak 2	0.053	1.10E-05	-0.12	0.023	3.07E-06	0.12

6.5 Strain Experiment

In the stain experiment, the whole fiber length is 450m and the whole fiber is under strain. The input power is 87mW which is relatively high as the fiber length is much shorter than that in the temperature experiment and there is no optical amplifier

available for 1319nm wavelength. The power monitored at the detector is 34μw. The result for the peak frequency of the first two peaks is demonstrated in fig 6.7. When the strain is less than 1475.6με, the peak frequencies almost remain constant. However, when the strain is larger than 1475.6με, the peak frequencies are increasing with increasing strain. This is due to the different mode coupling between acoustic mode and the optical mode when the strains are applied.

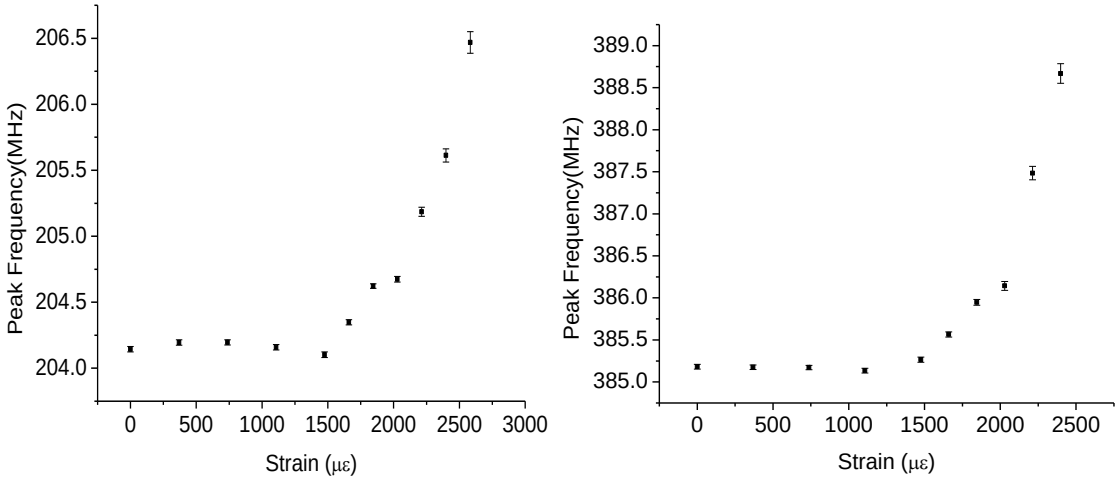

Fig 6. 7. The relationship of peak frequencies of peak 1 and peak 2 with strain.

In chapter 4, for the BOTDA system the measured strain coefficients for peak 1 and peak 2 were the same. That means that they may have the same variation tendency before 1475.6με. After this point, they alter differently with higher strain applied. Fig 6.8. shows the calculated frequency differences of peak 1-2 and peak 1-3 with increasing strain and it follows our analysis.

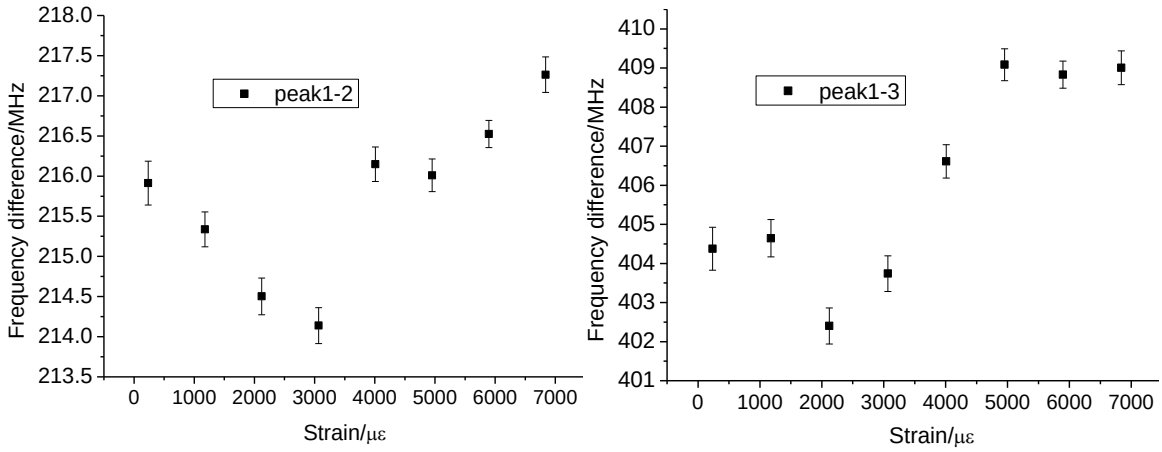

Fig 6. 8. The frequency difference of peak 1-2 and peak 1-3 with the strain: calculated from the results of the BOTDA system in chapter 4.

At the same time we also got the peak power's relationship with strain which is shown in fig 6.9. It can be seen that the peak power is decreasing with increasing strain, which is just the same behaviour as the first two peaks of LEAF fiber in chapter 4.

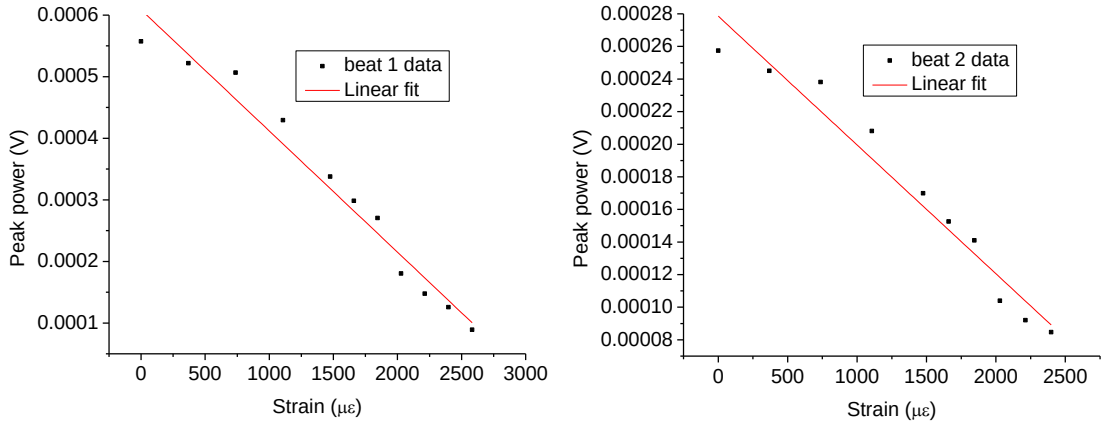

Fig 6. 9. The peak powers as a function of strain for the first two peaks.

As in the temperature experiment, we also explored the connection between the linewidth and strain in fig 6.10. Here, we found an unusual behaviour which was different from the peaks of LEAF fiber. It was demonstrated in chapter 4 that the linewidths of

LEAF fiber's Brillouin peaks were decreasing with increasing strain. For the LEAF beat spectrum, the first two peaks' linewidth didn't change before 1475.6με. When the strain is higher than this value, the linewidth was increased. This behaviour is similar with the peak frequency and it is also induced by the coupling effect between different acoustic modes.

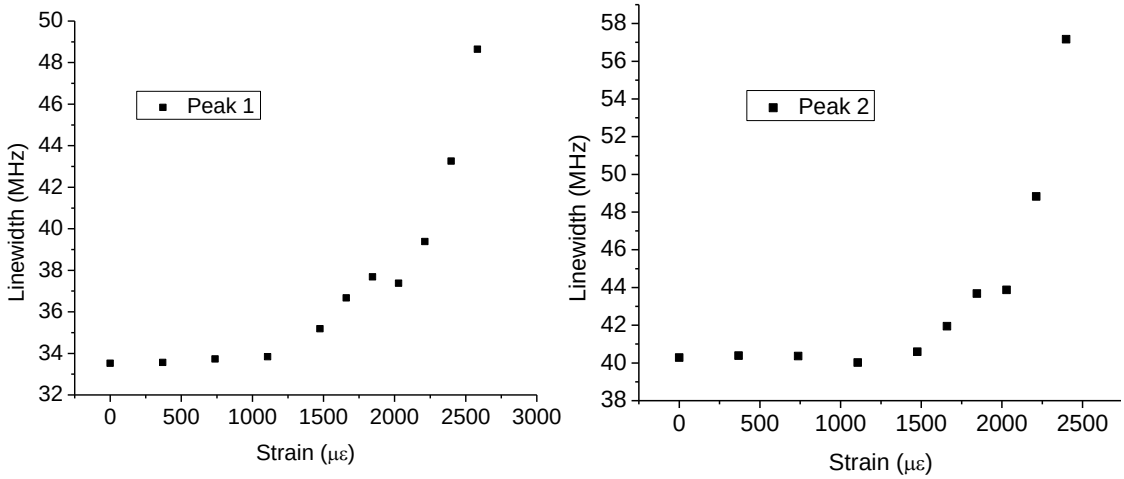

Fig 6. 10. The first two peaks' linewidth as a function of strain.

According to the peak frequency and linewidth's different behaviour around 1475.6με, we divide the strain into two parts: one is less than 1475.6με while the other is larger than 1475.6με. For the second part, the peak frequency and linewidth can be fitted linearly with strain. Therefore, in the first part, the coefficients between linewidth/peak frequency and strain are zero. We can use the peak power's linear relationship with strain to get the strain variation value. Thus the temperature and strain can be discriminated. In the second part, we can just use the normal simultaneous temperature and strain discrimination method applying the peak frequency or linewidth with peak power. Table

6.4 and table 6.5 show the fitted coefficients and uncertainties for peak frequency, peak power and linewidth.

Table 6. 4. The coefficients and uncertainties for the linear fit of peak frequency, peak power and linewidth when the strain is less than 1475.6με.

	$C_\varepsilon(V_B)$ (MHz/με)	$C_\varepsilon(P)$ (V/με)	$C_\varepsilon(W)$ (MHz/με)	$\delta_{VB}(\varepsilon)$ (MHz)	$\delta_p(\varepsilon)$ (V)	$\delta_W(\varepsilon)$ (MHz)
Peak 1	0	-1.97E-07	0	0.02	2.21E-06	0.11
Peak 2	0	-7.90E-08	0	0.03	1.14E-06	0.15

Table 6. 5. The coefficients and uncertainties for the linear fit of peak frequency, peak power and linewidth when the strain is larger than 1475.6με.

	$C_\varepsilon(V_B)$ (MHz/με)	$C_\varepsilon(P)$ (V/με)	$C_\varepsilon(W)$ (MHz/με)	$\delta_{VB}(\varepsilon)$ (MHz)	$\delta_p(\varepsilon)$ (V)	$\delta_W(\varepsilon)$ (MHz)
Peak 1	0.00218	-1.97E-07	0.01	0.04	2.21E-06	0.25
Peak 2	0.0042	-7.90E-08	0.016	0.06	1.14E-06	0.42

6.6 Calculation Result - Simultaneous Temperature and Strain Discrimination

The relationships between peak frequency and peak power with temperature and strain can be expressed as

$$\begin{bmatrix} \Delta\nu_B^{pki} \\ \Delta P^{pki} \end{bmatrix} = \begin{bmatrix} C_{\upsilon\varepsilon}^{pki} & C_{\upsilon T}^{pki} \\ C_{p\varepsilon}^{pki} & C_{pT}^{pki} \end{bmatrix} \begin{bmatrix} \Delta\varepsilon \\ \Delta T \end{bmatrix} \tag{6.2}$$

Thus, the maximum strain and temperature errors can be written as [61]

$$\delta T = \frac{\left|C_\varepsilon^p\right|\delta\nu_B + \left|C_\varepsilon^{\nu_B}\right|\delta p}{\left|C_T^p C_\varepsilon^{\nu_B} - C_\varepsilon^p C_T^{\nu_B}\right|} \tag{6.3}$$

$$\delta\varepsilon = \frac{\left|C_T^p\right|\delta\nu_B + \left|C_T^{\nu_B}\right|\delta p}{\left|C_T^p C_\varepsilon^{\nu_B} - C_\varepsilon^p C_T^{\nu_B}\right|} \tag{6.4}$$

When the strain is less than 1475.6με, the equations (6.3) and (6.4) can be transformed into (6.5) and (6.6)

$$\delta T = \frac{\left|C_\varepsilon^p\right|\delta\nu_B}{\left|C_\varepsilon^p C_T^{\nu_B}\right|} \tag{6.5}$$

$$\delta\varepsilon = \frac{\left|C_T^p\right|\delta\nu_B + \left|C_T^{\nu_B}\right|\delta p}{\left|C_\varepsilon^p C_T^{\nu_B}\right|} \tag{6.6}$$

For linewidth and peak power, using the same method similar equations could also be acquired. When the strain is less than 1475.6με, the maximum strain and temperature error using both of these methods is shown in table 5.6. The smallest strain and temperature errors are obtained for peak 2 which are 93με and 0.4°C respectively.

Table 6. 6. The calculated temperature and strain error: strain less than 1475.6με

	Peak frequency & Peak power		Linewidth & Peak power	
	S-error (με)	T-error (℃)	S-error (με)	T-error (℃)
Peak 1	102	0.6	121	0.67
Peak 2	93	0.4	188	1

When the strain is larger than 1475.6με, equations (6.3) and (6.4) can be directly used. Table 6.7 shows the calculated temperature and strain errors. The smallest temperature and strain errors are 14με and 0.3°C for peak 2. These errors are relatively small because the central frequency shift has the same change tendency for both strain and temperature while the peak power has different signs. In this way the temperature and strain error is decreased which is just the same principle as in [67].

Table 6. 7. Calculated strain and temperature errors: strain larger than 1475.6με

	Peak frequency & Peak power		Linewidth & Peak power	
	S-error (με)	T-error (℃)	S-error (με)	T-error (℃)
Peak 1	17.7	0.3	29	0.38
Peak 2	14	0.3	28	0.35

It seems that peak 2 has a better result than peak 1, because of the larger difference between peak 1/peak 3 and peak 1/peak 2 of LEAF fiber's four peaks. Hence, the variations of LEAF beat's peak 2 have larger temperature and strain dependence than peak 1. Although the method of using linewidth and peak power produced larger temperature and strain error than applying the peak frequency and peak power for the discrimination, the absolute value of the slope for linewidth in the temperature experiment is larger than the peak frequency. This means, using the linewidth and peak power detection method will produce a higher accuracy. Therefore, when the strain is larger than 1475.6με this method could be adopted.

6.7 Conclusion

We have shown that temperature and strain can be measured simultaneously in LEAF fiber from the measurement of the peak power, peak frequency and linewidth of the beat spectrum's first two peaks. The best temperature and strain errors we can get are 0.4°C and 93με when the applied strain is less than 1475.6με while the results are 0.3 ℃ and 14με when the strain is larger than 1475.6με. Therefore, it should be feasible to construct a fully distributed temperature and strain sensor using this method.

Chapter 7

Conclusion

7.1 Thesis Outcomes

My research is focused on the characterization of LEAF fiber's Brillouin spectrum so as to explore its potential for use as a distributed temperature and strain sensor.

A frequency square law was widely used to describe the Brillouin linewidth's dependence on wavelength. In order to verify this rule in LEAF fiber, we performed the spontaneous Brillouin scattering experiment at wavelengths of 1319 and 1550 nm. The result showed that the third and fourth peaks of LEAF fiber don not satisfy the frequency square law. For comparison, we also did the same experiment on SMF-28^{TM}. This fiber confirmed the frequency square law as reported. From these two fiber's behaviour, it is inferred that the frequency squared law may not be correct in fibers where there is acoustic waveguide. Therefore, a more complete model is needed to describe the frequency dependence of the spectral width for Brillouin scattering in optical fibers.

In the stimulated Brillouin scattering regime, we studied the temperature and strain characteristics of LEAF fiber's Brillouin spectrum such as the peak power, the Brillouin frequency shift and the Brillouin linewidth. Since LEAF fibers have four peaks, many interesting features were discovered. We found that when the strain increases the first two

peaks' peak power will decrease while the third and fourth peaks' peak power do not change, and the four peaks' linewidth will all decrease. The latter one is a new feature which is different from the standard SMF whose linewidth remains constant when the strain increases. When temperature increases the four peaks' peak power will have a quadratic dependence on temperature, and their linewidth decreases with increasing temperature. The linewidth's behavior in the temperature range is similar to SMF. A simultaneous temperature and strain sensor was also explored based on the linear relation between the Brillouin frequency shift/linewidth and temperature/strain. We achieved a strain error of 37με and temperature error of 1.8°C with a spatial resolution of 4m for the first peak.

The polarization's effect in the process of Brillouin scattering is not only on the Brillouin gain but also on the Brillouin frequency shift. In the spontaneous regime, we demonstrated experimentally that the variation of the input SOP changes the Brillouin frequency shift and the Brillouin linewidth of the four peaks for LEAF fiber. The Brillouin frequency is shifted by 0.2MHz for the first three peaks in the Stokes case while for the anti-Stokes case the average Brillouin frequency shift is 0.2-0.4 MHz. According to the probability density histograms of the four peaks in the Stokes and anti-Stokes cases, the four peaks's Brillouin frequency shift have larger dependence on the SOP change of the input light in the Stokes case. The first peak has the highest dependence on the input light's SOP change in both the Stokes and anti-Stokes cases.

We discovered the LEAF beat spectrum which was caused by the beating between the first peak and the other peaks of the LEAF fiber. This occurred when the input power

is relatively high: several mW. At this time, the first peak of LEAF fiber has enough energy to beat with the rest of the peaks. We used the first two peaks of LEAF beat for the temperature and strain sensor applying the linear relationship between peak power/peak frequency/linewidth and temperature/strain. The best temperature and strain resolutions we obtained are 0.4°C and 93με when the applied strain is less than 1475.6με while the results are 0.3°C and 14με when the strain is larger than 1475.6με. 1475.6με is a critical point which is associated with the fiber length. This provided a probability to construct a fully distributed temperature and strain sensor.

7.2 Future Work

The Brillouin linewidth ratio's dependence on temperature and power level is also interesting to be examined since the linewidth changes with temperature and power level. These should have some influence in the linewidth ratio for different wavelength.

In order to achieve better temperature and strain resolution in LEAF fiber using the BOTDA system, the same experiment is worthwhile to be tried on the 1550nm system. Moreover, to improve the spatial resolution, a shorter pulse width could be adopted.

The probability histograms in both the Stokes and anti-Stokes cases were drawn for the Brillouin peak frequency. It would be valuable to see what kind of distribution they meet with. Although they don't satisfy the Maxwellian distribution, a similar distribution for the Brillouin frequency shift should be expected.

We did the temperature and strain experiment for LEAF beat separately and

estimated the maximum temperature and strain error. Although the third peak of LEAF beat has lower peak power than the first two peaks, it is still worthwhile to try the simultaneous temperature and strain measurements using this peak as this peak may have a larger dependence on temperature and strain. For a real simultaneous temperature and strain sensor, it would be possible to apply the temperature and strain at the same position in the fiber. To achieve a distributed temperature and strain sensor, a short pulse instead of the CW wave could be applied so as to get the spatial information. Using the oscilloscope we can get the spectrum without sweeping the frequency, which was commonly applied in BOTDA and BOTDR. As a result, the system configuration will be largely simplified and the total cost will be hugely reduced for distributed Brillouin sensors.

Reference

[1] Andrey Kobyakov, Michael Sauer, and Dipak Chowdhury, “Stimulated Brillouin scattering in optical fibers”, Adv. Opt. Photon. 2, 1-59 (2010).

[2] S. K. Yao and C. K. Asawa, “Fiber Optical Intensity Sensors”, IEEE J. of Sel. Areas in Communication, SAC-1(3), 1983.

[3] N. Lagokos, L. Litovitz, P. Macedo, and R. Mohr, “Multimode Optical Fiber Displacement Sensor”, Appl. Opt., Vol. 20, p. 167, 1981.

[4] B.Glisic, D.Inaudi, and N.Casanova, “SHM process as perceived through 350 projects,” in Smart Struct. Mater. /NDE Symp., SanDiego, CA, 2010, p.76480P.

[5] J.M.López-Higuera, Optical Sensors. Cantabria, Spain: Universidad de Cantabria, 1998.

[6] R.H.West, H.Buker, E.J.Friebele, H.Henschel, and P.B.Lyons. “The use of optical-time domain reflectometers to measure radiation-Induced losses in optical fibers,” J. LightwaveTechnol., vol. 12, no.4, pp. 614–620, Apr.1994.

[7] D.Culverhouse, F.Farahi, C.N.Pannell, and D.A.Jackson, “Potential of stimulated Brillouin-scattering as sensing mechanism for distributed temperature sensors,” Electron. Lett., vol. 25, no.14, pp. 913–915, Jul.1989.

[8] M.-J. Li, X. Chen, J. Wang, A. B. Ruffin, D. T. Walton, S. Li, A. Nolan, S. Gray, and

L. A. Zenteno, “Fiber designs for reducing stimulated Brillouin scattering,” in Optical Fiber Communication Conference and National Fiber Optic Engineers Conference, Technical Digest (CD) (Optical Society of America, 2006), paper OTuA4.

[9] Agrawal, G.p., Nonlinear Fiber Optics (Academic Press, Boston, 1989)

[10] A. Kobyakov, S. Kumaro, D. Q. Chowdhury, A. B. Ruffin, M. Sauer, S. R. Bickham, and R. Mishra, "Design concept for optical fibers with enhanced SBS threshold", Opt. Exp. vol. 13, No. 14, pp. 5338-5346 (2005).

[11] Y. Koyamada, S. Sato, S. Nakamura, H. Sotobayashi, and W. Chujo, "Simulating and designing Brillouin gain spectrum in single mode fibers", J Lightwave Technol., vol. 22, pp. 631-639, 2004.

[12] A. Boh Ruffin, Ming-Jun Li, Xin Chen, Andrey Kobyakov, and Frank Annunziata, "Brillouin gain analysis for fibers with different refractive indices," Opt. Lett. 30, 3123-3125 (2005)

[13] Horiguchi. T, Shimizu. K, Kurashima. T, Tateda. M., Koyamada.Y, “Development of a Distributed Sensing Technique Using Brillouin Scattering, ” J. Lightwave Technol. 1995,13, 1296-1302.

[14] D. Garus, F. Schliep, K. Krebber, and T. Golgolla, “Distributed Sensing Technique Based on Brillouin Optical Fiber Frequency Domain Analysis,” Optics Letters, 21, 1402-1404 (1996).

[15] D. Garus, T. Golgolla, K. Krebber, and F. Schliep, “Brillouin optical frequency domain analysis for distributed temperature and strain measurements,” IEEE Journal of

Lightwave Technology, 15, 654-662 (1997).

[16] Hotate. K, Hasegawa. T. “Measurement of Brillouin gain spectrum distribution along an optical fiber with a high spatial resolution using a correlation based technique”, Proposal, experiment and simulation. IEICE Trans. Electron. 2000, E83-C, 405-411.

[17] Hotate. K, Tanaka. M. “Distributed fiber Brillouin strain sensing with 1cm spatial resolution by correlation based continuous wave Technique”. IEEE Photonic. Technol. Lett. 2002, 14, 179-181.

[18] Song. K.Y., Hotate.K, “Distributed Fiber Strain Sensor With 1-kHz Sampling Rate Based on Brillouin Optical Correlation Domain Analysis”. IEEE Photonic. Technol. Lett. 2007, 23, 1928-1930.

[19] Robert W. Boyd, “Nonlinear Optics-3rd Edition”, Academic Press (2008).

[20] Fabelinskii, I.L., 1968. “Molecular Scattering of Light”. Plenum Press, NewYork.

[21] Xiaoyi Bao, Liang Chen. “Recent progress in Brillouin scattering based fiber sensors”. Sensors 2011, 11, 4152-4187.

[22] E. P. Ippen, “Low‐power quasi‐cw raman oscillator”, Appl. Phys. Lett. 16, 303 (1970).

[23] R. H. Stolen, E. P. Ippen, and A. R. Tynes, “Raman Oscillation in Glass Optical Waveguide”, Appl. Phys. Lett. 20, 62 (1972).

[24] E. P. Ippen and R. H. Stolen, Paper F9, 7th International Quantum Electronics

Conference, Montreal, May 1972.

[25] R. G. Smith, “Optical power handling capacity of low loss optical fibers as determined by stimulated Raman and Brillouin scattering”, Appl. Opt., 11, 2489-2494 (1972).

[26] N. G. R. Broderick, H. L. Offerhaus, D. J. Richardson, R. A. Sammut, J. Caplen, and L. Dong, “Large Mode Area Fibers for High Power Applications”, Optical Fiber Technology, vol. 5, 185-196 (1999)

[27] M. J. Li, S. Li and D. A. Nolan, "New Dispersion Decreasing Fiber with High SBS Threshold for Nonlinear Signal Processing",OFCNFOEC 2005, paper OFH5 (2005).

[28] P. D. Dragic, C.-H. Liu, G. C. Papen, and A. Galvanauskas, “Optical fiber with an acoustic guiding layer for stimulated Brillouin scattering suppression,” in Conference on Lasers and Electro-Optics/Quantum Electronics and laser Science and Photonic Applications Systems Technologies, Technical Digest (CD) (Optical Society of America, 2005), paper CTHZ3.

[29] A. Hadjifotiou and G.A. Hill, "Suppression of stimulated Brillouin backscattering by PSK modulation for high-power optical transmission," IEE Proc. J 133 256-258 (1986).

[30] L. Eskildsen, P.B. Hansen, U. Koren, B.I. Miller, M.G. Young, and K.F. Dreyer, "Stimulated Brillouin scattering suppression with low residual AM using a novel temperature wavelength-dithered DFB laser diode," Electron. Lett. 32, 1387-1389 (1996).

[31] Y.K. Chen, Y.L. Liu, and C.C. Lee, "Directly modulated 1.55 μm AM-VSB video EDFA-repeatered supertrunking system over 110km standard singlemode fibre using

split-band and wavelength division multiplexing techniques," Electron. Lett. 33, 1400-1401 (1997).

[32] N. Yoshizawa, T. Horiguchi, and T. Kurashima, "Proposal for stimulated Brillouin scattering suppression by fibre cabling," Electron. Lett. 27, 1100-1101 (1991).

[33] M. Ohashi and M. Tateda, "Design of a strain-free-fiber with nonuniform dopant concentration for stimulated Brillouin scattering suppression," J. Lightwave Technol. 11, 1941-1945 (1993).

[34] K. Shiraki, M. Ohashi, and M. Tateda, "Suppression of stimulated Brillouin scattering in a fibre by changing the core radius," Electron. Lett. 31, 668-669 (1995).

[35] D. Cotter, “Stimulated Brillouin scattering in optical fibers,” J. Opt. Commun., vol.4, pp.10–17, 1982.

[36] R.W.Tkach, A.R.Chraplyvy, and R.M.Derosier, “Spontaneous Brillouin scattering for single mode optical fiber characterization,” Electron. Lett., vol.22, pp.1011–1012, 1986.

[37] N.Shibata, R.G.Waarts, and R.P.Braun, “Identification of longitudinal acoustic modes guided in the core region of a single mode optical fiber by Brillouin gain spectra measurements,” Opt.Lett., vol.12, pp.595–597, 1986.

[38] S.Gray, D.T.Walton, X.Chen, J.Wang, M.-J.Li, A.Liu, A.B.Ruffin, J.A.Demeritt, and L.A.Zenteno, “Optical Fibers With Tailored Acoustic Speed Profiles for Suppressing Stimulated Brillouin Scattering in High-Power, Single-Frequency Sources”, J. Lightwave Technol. 15(2009)37–46.

[39] Benjamin G. Ward and Justin B. Spring, "Brillouin gain in optical fibers with inhomogeneous acoustic velocity", Proc. SPIE 7195, 71951J (2009).

[40] J. E. Masnik, J. Kieffer, and J. D. Bass, “Structural relaxations in alkali silicate systems by Brillouin light scattering,” J. Am. Ceram. Soc. 76(12), 3073–3080 (1993).

[41] O. L. Anderson, and H. E. Bömmel, “Ultrasonic absorption in fused silica at low temperatures and high frequencies,” J. Am. Ceram. Soc. 38(4), 125–131 (1955).

[42] J. Kieffer, “Mechanical degradation and viscous dissipation in B_2O_3.,” Phys. Rev. B Condens. Matter 50(1), 17–29 (1994).

[43]D. Heiman, D. S. Hamilton, and R. W. Hellwarth, “Brillouin scattering measurements on optical glasses”, Phys. Rev. B 19, 6583–6592 (1979)

[44]C. Krischer, “Optical measurements of ultrasonic attenuation and reflection losses in fused silica,” J. Acoust. Soc. Am. 48(5B), 1086–1092 (1970).

[45] Y.Azuma, N.Shibata, T.Horiguchi, and M.Tateda, “wavelength dependence of Brillouin-gain spectra for single-mode optical fibres” Electron. Lett. 24, 250 (1988).

[46] Pi-Cheng Law and Peter D. Dragic, "Wavelength dependence of the Brillouin spectral width of boron doped germanosilicate optical fibers," Opt. Express 18, 18852-18865 (2010).

[47] Rongqing Hui, Maurice O’Sullivan, Fiber Optic Measurement Techniques (Elsevier Academic Press, 2009).

[48]Fabien Ravet, Xiaoyi Bao, Jeff Snoddy, Yun Li, Liang Chen, "Characterization of Brillouin fiber generator and amplifier for optimized working condition of the distributed sensors" Opt. Fiber Technology. 15, 304-309 (2009).

[49] Guanshi Qin, Takenobu Suzuki, and Yasutake Ohishi, "Power dependence of Brillouin linewidths in a silica fiber," Opt. Lett. 32, 3155-3157 (2007)

[50] P.J. Thomas, N.L. Rowell, H.M. van Driel, and G.I. Stegeman, "Normal acoustic modes and Brillouin scattering in single-mode optical fibers," Phys. Rev. B 19, 4986-4998 (1979).

[51] Peter D. Dragic, "Tailoring of the Brillouin gain profile for fiber-based sensor systems and networks", Proc. SPIE 7316, 731607 (2009); doi:10.1117/12.818817

[52] T.Horiguchi, T.Kurashima, and M.Tateda,"Tensile strain dependence of Brillouin frequency shift in silica optical fibers," Photon. Technol. Lett. 1, 107–108 (1989).

[53] D.Culverhouse, F.Farahi, C.N.Pannell, and D.A.Jackson, "Potential of stimulated Brillouin scattering as sensing mechanism for distributed temperature sensors ," Electron.Lett. 25, 913–915 (1989).

[54] Jeff Smith, Anthony Brown, Michael DeMerchant, and Xiaoyi Bao, "Simultaneous Distributed Strain and Temperature Measurement," Appl. Opt. 38, 5372-5377 (1999)

[55] Lufan Zou, Graham A. Ferrier, Shahraam Afshar V., Qinrong Yu, Liang Chen, and Xiaoyi Bao, "Distributed Brillouin Scattering Sensor for Discrimination of Wall-Thinning Defects in Steel Pipe under Internal Pressure," Appl. Opt. 43, 1583-1588 (2004)

[56] X.Bao, D.J.Webb, and D.A.Jackson, “Combined distributed temperature and strain sensor based on Brillouin loss in an optical fiber,” Opt. Lett. 19, 141–143 (1994)

[57] T. R. Parker, M. Farhadiroushan, V. A. Handerek, and A. J. Rogers, “Temperature and strain dependence of the power level and frequency for spontaneous Brillouin scattering in optical fibers”, Opt. Lett., vol. 22, no. 11, pp.787 - 789 , 1997.

[58] T.R.Parker, M.Farhadiroushan, R.Feced, and V.A.Hand-erek, “Simultaneou distributed measurement of strain and temperature from noise-initiated Brillouin scattering in optical fibers,” Quantum Electron.34, 645–659 (1998).

[59] Huai H. Kee, Gareth P. Lees, and Trevor P. Newson, “All-fiber system for simultaneous interrogation of distributed strain and temperature sensing by spontaneous Brillouin scattering,” Opt. Lett. 25, 695-697 (2000)

[60] C. C. Lee, P. W. Chiang, and S. Shi, “Utilization of a dispersion-shifted Fiber for simultaneous measurement of distributed strain and temperature through Brillouin frequency shift,” IEEE Photon. Technol. Lett. 13, 1094-1096 (2001).

[61] M.Alahbabi, Y.Y.Cho, and T.P.Newson, “Comparison of the methods for discriminating temperature and strain in spontaneous Brillouin-based distributed sensors,” Opt. Lett. 29, 26-28 (2004).

[62] L. Zou, X. Bao, S. Afshar, and L. Chen, “Dependence of the Brillouin frequency shift on strain and temperature in a photonic crystal fiber,” Opt. Lett. 29, 1485-1487 (2004).

[63] X. Bao, Q. Yu, and L. Chen, “Simultaneous strain and temperature measurements

with polarization-maintaining fibers and their error analysis by use of a distributed Brillouin loss system," Opt. Lett. 29, 1342-1344 (2004).

[64] W. Zou, Z. He, M. Kishi, and K. Hotate, "stimulated Brillouin scattering and its dependences on strain and temperature in a high-delta optical fiber with F-doped depressed inner cladding" Opt. Lett. 32, 600-602 (2007).

[65] W.Zou, Z.He, and K.Hotate, "Demonstration of Brillouin distributed discrimination of strain and temperature using a polarization-main-taining optical fiber," IEEE Photon.Technol. Lett., vol. 22, no.8, pp.526–528, Apr.15,2010.

[66] Yongkang Dong, Liang Chen, and Xiaoyi Bao, "High-spatial-resolution simultaneous strain and temperature sensor using Brillouin scattering and birefringence in a polarization-maintaining fibre", IEEE PTL, 22, 1364-1366 (2010)

[67] Weiwen Zou, Zuyuan He, and Kazuo Hotate, "Complete discrimination of strain and temperature using Brillouin frequency shift and birefringence in a polarization maintaining fiber," Opt. Express 17, 1248-1255 (2009)

[68] Govind P.Agrawal, Fiber-optic Communication Systems, 3rd edition, chapter 2.

[69] Sergey Akopov and John Jay, "BOTDR Measurements of Corning Single-Mode Optical Fibers", Corning Optical Fiber white papers, May 2010

[70] Hao Liang, Wenhai Li, Nicolas Linze, Liang Chen, and Xiaoyi Bao, "High-resolution DPP-BOTDA over 50 km LEAF using return-to-zero coded pulses," Opt. Lett. 35, 1503-1505 (2010)

[71] Yongkang Dong, Xiaoyi Bao, and Wenhai Li, "Differential Brillouin gain for improving the temperature accuracy and spatial resolution in a long-distance distributed fiber sensor," Appl. Opt. 48, 4297-4301 (2009)

[72] J.P.Smith, “Characterisation of the Brillouin Loss Spectrum for Simultaneous Distributed Sensing of Strain and Temperature,” M.S. thesis, The University of New Brunswick (1999).

[73] Davis, C.C. Lasers and Electro-optics, (Cambridge University, Cambridge, 1996)

[74] Timoshenko, S.P., and J.Goodier, Theory of Elasticity, 3rd Edition, (McGraw-Hill Inc., New York, 1970).

[75] M. Nikles, L. Thévenaz, and P. Robert, "Brillouin gain spectrum characterization in single-mode optical fibers," J. Lightwave Technol. 15, 1842-1851 (1997).

[76] Jen,C.K.,1985. “Similarities and differences between fiber acoustics and fiber optics”. Proceedings of the IEEE Ultasonics Symposium: 1128-1133.

[77] Nori Shibata, Katsunari Okamoto, and Yuji Azuma, "Longitudinal acoustic modes and Brillouin-gain spectra for GeO2-doped-core single-mode fibers," J. Opt. Soc. Am. B 6, 1167-1174 (1989)

[78] Dugas, J., P. Michel, L.Martin, and J.M. Cariou, “Behavior of the refractive index and of the coefficient of thermal expansion of silicone with temperature,” Appl. Opt. 25, 3807-3808(1986)

[79] Li, H. H., “Refractive index of Silicon and Germanium and its wavelength and

temperature derivatives," J. Phys. Chem. Ref. Data 9, 561-601 (1980).

[80] J.D.C. Jones, in Optical Fiber Sensors, Vol.16 of 1997 OSA Technical Digest Series (Optical Society of America, Washington, D.C., 1997, p.36.

[81] C.D.Poole and J.Nagel,"Polarization effects in lightwave systems," in Optical Fiber Telecommunications IIIA, I. P. Kaminow and T.Koch, eds., Academic Press (1997).

[82] B.W. Hakki, " Polarization mode dispersion in a single mode fiber," Journal of Lightwave Technology, vol. 14, no. 10, pp. 2202-2208, 1996

[83] Shangran Xie, Xiaoyi Bao and Liang Chen, "Distributed fiber beat length, birefringence and differential group delay measurement using BOTDA technique", Proc. SPIE 7753, 7753A6 (2011);

[84] Xiaoyi Bao, Jesse Leeson, Jeff Snoddy and Liang Chen (2009). "Fiber Sensor Applications in Dynamic Monitoring of Structures, Boundary Intrusion, Submarine and Optical Ground Wire Fibers", Optical Fiber New Developments.

[85] Waddy, D.S, Chen, L, Bao, X. "Polarization effects in aerial fibers". Opt. Fiber Technol., Vol.11, No.1, 2005(1-19)

[86] Zhang, Z, Bao, X, Yu, Q, Chen, L. "Fast states of polarization and PMD drift in submarine fibers". Photon. Technol. Lettt., Vol. 18, No. 9, 2006(1034-1036).

[87] Leeson, J; Bao X; Cote, A. "Polarization Dynamics in Optical Ground Wire (OPGW) Network". Appl. Opt., Vol.48, No.14, 2009(2214-2219).

[88] M. O. Deventer and A. J. Boot, “Polarization properties of stimulated Brillouin scattering in single-mode fibers,” J. Lightwave Technol., vol. 12, p.585, 1994.

[89] Bao, X.; Dhliwayo, J.; Heron, N.; Webb, D.J.; Jackson, D.A. “Experimental and theoretical studies on a distributed temperature sensor based on Brillouin scattering”. J. Lightwave Technol. 1995, 13, 1340-1348.

[90] Tsuneo Horiguchi and Mitsuhiro Tateda, “Optical-fiber-attenuation investigation using stimulated Brillouin scattering between a pulse and a continuous wave,” Opt. Lett. 14, 408-410 (1989)

[91] A. Zadok, A. Eyal, M. Tur and L. Thévenaz. “Polarization attributes of stimulated Brillouin scattering slow light in fiber”. Photonics West - Advances in Slow and Fast Light IV, San Francisco, California, USA, 23 January 2011.

[92] Maughan, S.M.; Kee, H.H.; Newson, T.P. “57-km single-ended spontaneous Brillouin-based distributed fiber temperature sensor using microwave coherent detection”. Opt. Lett. 2001, 26, 331-333.

[93] Alahbabi, M.N; Cho, Y.T.; Newson, T.P. “150-km-range distributed temperature sensor based on coherent detection of spontaneous Brillouin backscatter and in-line Raman amplification”. J. Opt. Soc. Am. B 2005, 22, 1321-1324.

[94] Alahbabi, M.N.; Cho, Y.T.; Newson, T.P., Wait, P.C.; Hartog, A.H. “Influence of modulation instability on distributed optical fiber sensors based on spontaneous Brillouin scattering”, J. Opt. Soc. Am. B 2004, 21, 1156-1160.

[95] Kaoru Shimizu, Tsuneo Horiguchi, Yahei Koyamada, and Toshio Kurashima,

"Coherent self-heterodyne detection of spontaneously Brillouin-scattered light waves in a single-mode fiber," Opt. Lett. 18, 185-187 (1993).

[96] J. Geng, S. Staines, M. Blake, and S. Jiang, “Distributed fiber temperature and strain sensor using coherent radio-frequency detection of spontaneous Brillouin scattering,” Appl. Opt. 46, 5928-5932 (2007).

[97] Alahbabi, M., Cho, Y., & Newson, T. (2010). “100km distributed temperature sensor based on coherent detection of spontaneous Brillouin back-scatter”. Measurement Science and Technology, 15(8), 1544-1547.

[98] Benjamin Ward and Justin Spring, "Finite element analysis of Brillouin gain in SBS-suppressing optical fibers with non-uniform acoustic velocity profiles," Opt. Express 17, 15685-15699 (2009)

Publications

Xuan Liu and Xiaoyi Bao, "Simultaneous temperature and strain measurement with bandwidth and peak of the Brillouin spectrum in LEAF fiber", Proc. SPIE 7753, 775328 (2011); OFS 21.

Xuan Liu and Xiaoyi Bao, “Brillouin Spectrum in LEAF and Simultaneous Temperature and Strain Measurement”, Journal of Lightwave Technology, accepted for publication, Sep 2011;

Xiaoyi Bao, Shangran Xie, Xuan Liu and Liang Chen, “The non-uniformity and dispersion in SBS based fiber sensors”. 3rd Asia-Pacific Optical Fiber Sensors Conference, accepted for publication.